Steel and Composite Structures, *Vol. 33, No. 1* (*2019*) *143-162*
DOI: https://doi.org/10.12989/scs.2019.33.1.143

Numerical analysis of stainless steel-concrete composite beam-to-column joints with bolted flush endplates

Yuchen Song*, Brian Uy [a] and Jia Wang [b]

School of Civil Engineering, The University of Sydney, Sydney, NSW 2006, Australia

(*Received June 26, 2019, Revised August 1, 2019, Accepted August 13, 2019*)

Abstract. A number of desirable characteristics concerning excellent durability, aesthetics, recyclability, high ductility and fire resistance have made stainless steel a preferred option in engineering practice. However, the relatively high initial cost has greatly restricted the application of stainless steel as a major structural material in general construction. This drawback can be partially overcome by introducing composite stainless steel-concrete structures, which provides a cost-efficient and sustainable solution for future stainless steel construction. This paper presents a preliminary numerical study on stainless steel-concrete composite beam-to-column joints with bolted flush endplates. In order to ensure a consistent corrosion resistance within the whole structural system, all structural steel components were designed with austenitic stainless steel, including beams, columns, endplates, bolts, reinforcing bars and shear connectors. A finite element model was developed using ABAQUS software for composite beam-to-column joints under monotonic and symmetric hogging moments, while validation was performed based on independent test results. A parametric study was subsequently conducted to investigate the effects of several critical factors on the behaviour of composite stainless steel joints. Finally, comparisons were made between the numerical results and the predictions by current design codes regarding the plastic moment capacity and the rotational stiffness of the joints. It was concluded that the present codes of practice generally overestimate the rotational stiffness and underestimate the plastic moment resistance of stainless steel-concrete composite joints.

Keywords: steel-concrete composite structure; stainless steel; beam-to-column joint; bolted flush endplate connection; finite element analysis; parametric study; design code

1. Introduction

The application of stainless steel in construction has witnessed steady growth in the past few decades. Compared with conventional carbon steel, stainless steel has significant advantages such as better durability and corrosion resistance, higher fire performance and ductility, as well as excellent recyclability and sustainability. Moreover, the architectural aesthetics is another benefit that promotes the use of stainless steel in iconic buildings and structures. Although the initial cost of stainless steel should be typically higher than carbon steel, the considerably lower maintenance requirements can make stainless steel an attractive option when the life-cycle costing of structures is a major concern.

A more recent trend of utilising stainless steel in structural engineering is to introduce composite action between stainless steel and concrete, namely the stainless steel-concrete composite (SSCC) structural system. Besides the superior features as stated above utilizing stainless steel, SSCC structures can partially overcome some of the main drawbacks of pure stainless steel (SS) structures. For example: (1) the total initial cost of SS structures can be significantly saved by reducing the amount of stainless steel used; (2) much higher strength can be achieved through composite actions therefore allowing stainless steel to be used in heavier applications; (3) instability issues (local and global buckling) of SS members can be largely eliminated by the restraint of concrete. Practical examples of SSCC structures include the composite beams of Cala Galdana Bridge in Spain, and the 115 m tall concrete-filled tubular towers of Stonecutters Bridge in Hong Kong, China.

In a SSCC structural system, reliable connections between SSCC beams and columns are of critical importance to ensure a robust overall structural behaviour. Concerning this application, welded and bolted connections are the two possible solutions. Although welded connections possess high strength and initial stiffness, they are not quite suitable for on-site connections as special treatments and techniques are generally required for stainless steel to reduce the risk of corrosion at the welds. On the other hand, the bolted solution is obviously more efficient and economic. Moreover, the corrosion issue can be eliminated by using stainless steel fasteners with equal or higher corrosion resistance than the connected parts. Among different types of bolted connections, the flush endplate connection is a commonly used configuration for composite beam-to-column joints due to its simplicity and preferred structural behaviour, which is the option considered in this study.

During the past few decades, a great deal of effort has

*Corresponding author, Ph.D. Candidate,
E-mail: yuchen.song@sydney.edu.au
[a] Ph.D., Professor, Head of School
[b] Ph.D., Research Associate

http://www.techno-press.org/?journal=scs&subpage=6
ISSN: 1229-9367 (Print), 1598-6233 (Online)

been devoted to research on carbon steel (CS)-concrete composite beam-to-column joints. For composite joints with I-section columns, Xiao *et al*. (1994) tested 20 specimens under symmetric and asymmetric monotonic loadings with different connection details. Similar works were carried out by Anderson and Najafi (1994) and Liew *et al*. (2000) on composite joints with endplate connections. Antisymmetric and cyclic loading tests were conducted by Simoes *et al*. (2001), Dubina *et al*. (2002), Liew *et al*. (2004), Salvatore *et al*. (2005), Vasdravellis *et al*. (2009) and Xiao *et al*. (2017). Concrete encased I-section columns were incorporated in the tests by Liew *et al*. (2000), Simões da Silva *et al*. (2001), Salvatore *et al*. (2005), and Vasdravellis *et al*. (2009). It was proved that the concrete encasement in the panel zone can be treated equivalent to stiffeners, which restricts the local buckling and excessive deformation of the column web and flange. Shanmugam *et al*. (2002) investigated the behavior of composite joints with haunched beams, which possess enhanced capacity and stiffness compared with conventional composite joints. Regarding composite joints with hollow and concrete-filled steel tubular (CFST) columns, monotonic loading tests were conducted by Loh *et al*. (2006a), Thai *et al*. (2017a), Wang *et al*. (2018a) and Waqas *et al*. (2019), while cyclic loading tests were carried out by Mirza and Uy (2011), Agheshlui *et al*. (2017), Wang *et al*. (2018a) and Waqas *et al*. (2019). Loh *et al*. (2006a, b) investigated the effects of shear connection degree on the behaviour of composite joints. It was concluded that the decrease in shear connection generally enhances the rotation capacity despite a slight decrease in the moment capacity.

Regarding SS bolted connections, investigations were performed by Salih *et al.* (2010, 2011, 2013) and Cai and Young (2014, 2018, 2019), which focus on SS spliced connections failed by shear. More recently, experimental studies were reported by Elflah *et al*. (2019a, b, c) and Hasan *et al.* (2019) on bolted beam-to-column joints built up with austenitic SS sections and bolts, as well as Yuan *et al.* (2019) on bolted T-stubs made with austenitic and duplex stainless steels. A numerical study was conducted by Wang *et al*. (2019) on extended endplate connections between SS beams and concrete-filled SS tubular columns. From the available investigations, SS beam-to-column joints show much higher ductility than carbon steel joints, corresponding with very large deformations in SS components. Through an assessment of the existing design code (CEN 2005), which was originally proposed for CS joints, it was concluded that the plastic moment resistance is underestimated by 34% to 44% for SS joints (Elflah *et al.* 2019a), mainly due to the remarkable strain-hardening nature of SS material. Blind bolted composite joints with concrete-filled SS tubular columns were investigated by Tao *et al.* (2017) and Song *et al.* (2017) and a review was presented by Han *et al*. (2019). However, since only columns are made of stainless steel in these works, the behaviour should be more similar to carbon steel composite joints rather than SSCC joints. Up to date, there is still no published reports available regarding composite joints fully made of stainless steel, which greatly restricts the application of SSCC joints in construction. Specifically, it is still not clear whether the design rules for CS composite joints are applicable for designing SSCC joints, upon which detailed appraisals are required based on experimental and numerical investigations.

The main aim of this paper is to investigate the basic behaviour of SSCC beam-to-column joints via finite element (FE) analyses. In order to ensure a consistent corrosion resistance within the joint, all structural components including beams, columns, endplates, bolts, reinforcing bars and shear connectors were designed with austenitic stainless steel. Bolted flush endplate connections with I-section beams/columns and solid concrete slabs (without profiled decking) were adopted in this study, which is the basic configuration for composite joints as specified in the current design codes (CEN 2004, AS/NZS 2017). Although SS welding studs shall be the most common solution for shear connectors in practical applications, the properties of such components are not available in literature. Instead, M16 SS bolts were used as shear connectors in the present study. In addition to the significant advantage of demountability, it has been proofed in a number of studies (Kwon *et al*. 2010, Pavlović *et al*. 2013, Dai *et al*. 2015, Rehman *et al.* 2016) that bolted shear connectors show compatible performance to conventional welding studs. The general-purpose FE module ABAQUS/Explicit was employed to numerically model SSCC joints. The developed FE model was validated against independent experimental tests. Subsequently, a comprehensive parametric study was carried out to investigate the key factors influencing the moment-rotation response of SSCC joints. Based on the numerical results, the current design provisions (CEN 2004, 2005, AS/NZS 2017) were assessed in terms of predictions on the plastic moment resistance, initial stiffness and moment-rotation characteristic of SSCC joints.

2. Finite element modelling

2.1 Elements, interactions and boundary conditions

The FE model was developed based on the platform of ABAQUS. Double-sided beam-to-column joints under monotonic and symmetric hogging moments were considered in the analysis. The beams and columns were connected by flush endplates via three rows of bolts (six bolts). Due to symmetry, only one side of the joint with a half column was modelled, as shown in Fig. 1. The reinforcing bars were modelled with two-node truss (T3D2) elements while all other instances were modelled with eight-node linear reduced integration (C3D8R) brick elements. A reasonable element size was selected with local mesh refinement at the regions where concentrated stresses could be encountered (e.g., bolt holes, contact regions between the concrete slab and shear connectors). For plated members (e.g., endplate, beam flange and web in compression), number of elements through thickness need to be increased as justified in Section 2.3.

A general contact algorithm with “hard contact” nominal property (i.e., minimize the node penetration) and “penalty”

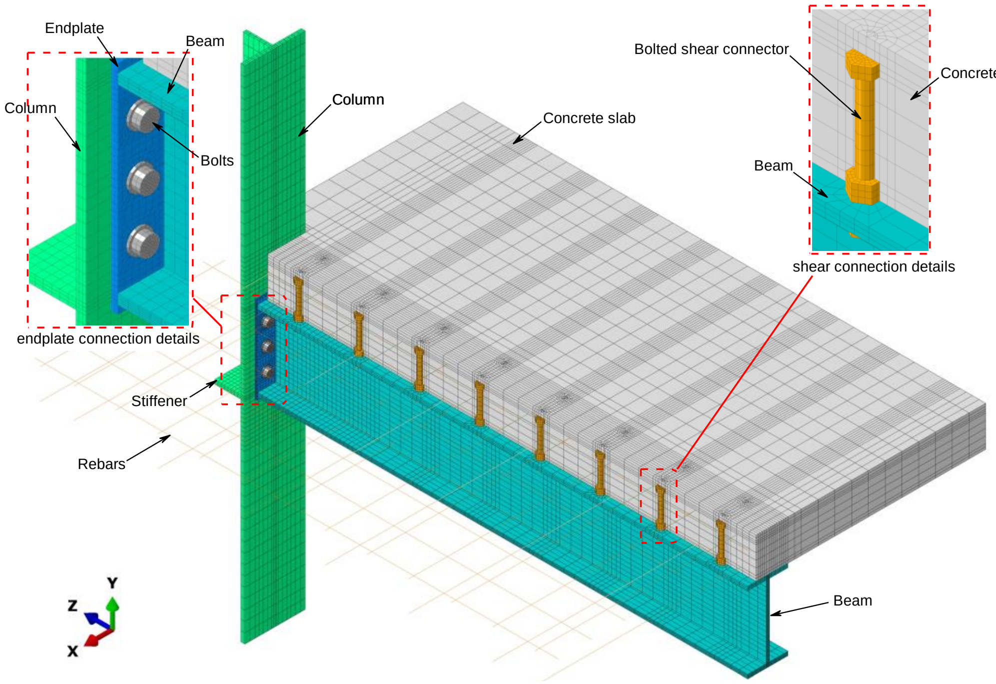

Fig. 1 FE model for SSCC beam-to-column joints (part of the concrete slab hidden)

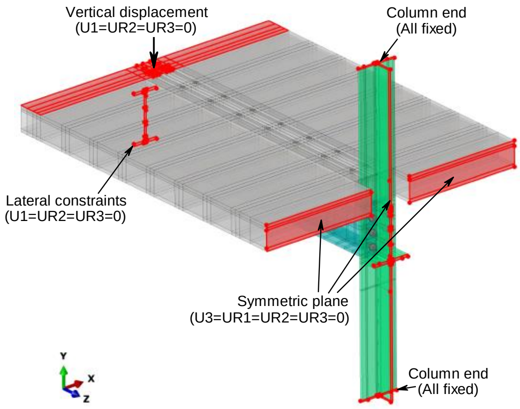

Fig. 2 Boundary conditions of the FE model

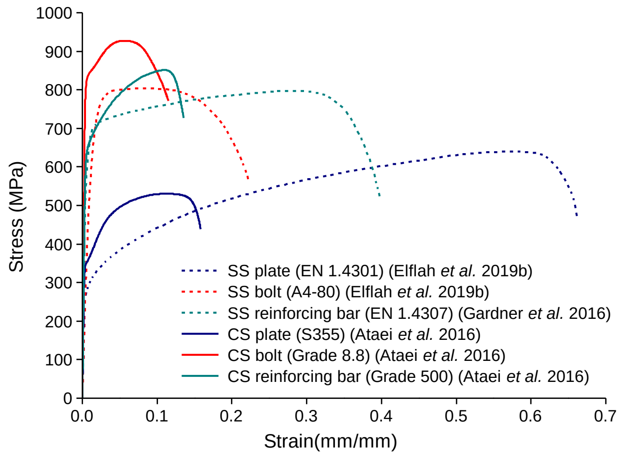

Fig. 3 Stress-strain curves of stainless and carbon steel components

tangential behaviour (a constant friction coefficient of 0.3) was defined to simulate all the contact pairs within the model. The transverse stiffeners and the endplate were tied to the column and the beam respectively, which is equivalent to welding connection. The reinforcing bars were embedded in the concrete slab by the "embedded region" constraint.

The load and boundary conditions of the model are

Table 1 Material properties of stainless and carbon steels

Material	Grade	Reference	Specimen	Elastic modulus E (MPa)	Yield stress f_y or $f_{0.2}$ (MPa)	Ultimate stress f_u (MPa)	f_u/f_y	Failure criterion (PEEQ)
SS	EN 1.4301	Elflah *et al*. (2019b)	Plate	201100	256	641	2.50	0.466
	EN 1.4307	Gardner *et al*. (2016)	Rebar	210200	562	796	1.42	0.303
	A4-80	Elflah *et al*. (2019b)	Bolt	191500	617	805	1.30	0.121
CS	S355	Ataei *et al*. (2016)	Plate	202000	352	523	1.49	0.099
	G500	Ataei *et al*. (2016)	Rebar	200000	610	854	1.40	0.115
	G8.8	Ataei *et al*. (2016)	Bolt	226000	837	926	1.11	0.074

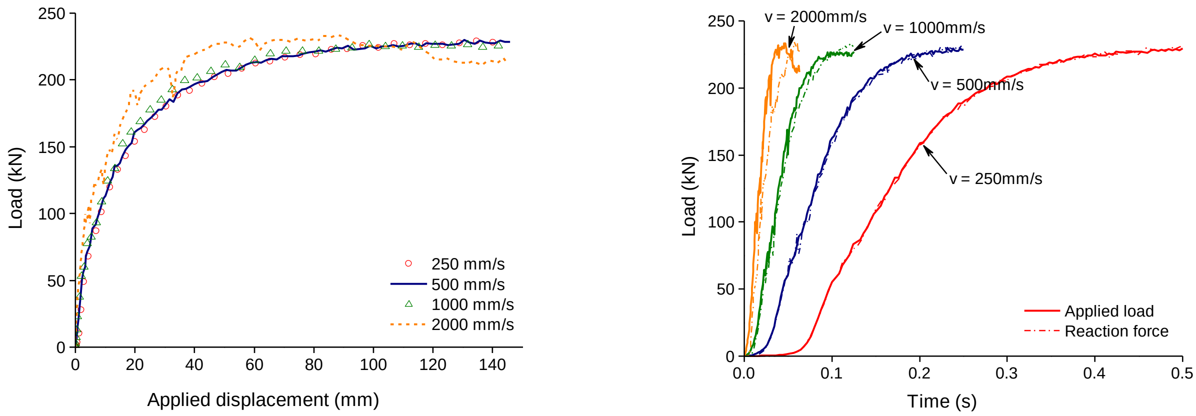

(a) Load-displacement responses (b) Applied load vs. reaction force

Fig. 4 Sensitivity of quasi-static explicit analysis to loading speed

shown in Fig. 2. Both ends of the column were fixed against all degrees of freedoms, while the symmetry constraint was applied to the identified symmetric plane. Lateral constraints were applied to the beam end to avoid lateral and torsional buckling modes. The bending moment was applied to the joint by deploying vertical displacement at the end of the slab. In order to prevent stress concentration on the slab, the vertical displacement was exerted through a reference point which was tied to an area on the slab surface as illustrated in Fig. 2.

2.2 Material properties

2.2.1 Steels

The material properties input for SS components were obtained from independent material test data in order to simulate the actual behaviour of SSCC joints. The SS plates (including beams, columns and endplates) are of austenitic grade EN 1.4301, while the SS bolts are of austenitic A4-80 grade for connecting beams and columns and as bolted shear connectors. Both properties were obtained from the tensile tests by Elflah *et al*. (2019b). It is noteworthy that the area of the bolt shank was taken as the stress area (CEN 2009) to consider the effects of threads. All longitudinal and transverse reinforcing bars are of austenitic grade EN 1.4307 with the tensile test data from Gardner *et al.* (2016).

In order for comparisons, composite joints with conventional CS materials were also modelled. The material properties were selected from Ataei *et al.* (2016), with comparable strength to the selected SS materials. A summary of the properties of the SS and CS materials is given in Table 1, while the stress-strain relationships are shown in Fig. 3. It is obvious that the SS materials possess higher level of strain hardening and ductility than the CS counterparts. Strain hardening of the SS plates is especially high with a relatively low yield strength (256MPa) and a large ultimate-to-yield strength ratio (2.50). Strain hardening effects of the SS reinforcing bars and bolts are less significant but still higher than the CS ones.

The engineering stress-strain relationships shown in Fig. 3 were converted to true plastic stress-strains in the FE model to obtain accurate simulation at large deformations. However, engineering stress-strain was input for the reinforcing bars as they were modelled by truss elements with constant cross section area. Failure of the steel components were defined based on equivalent plastic strain (PEEQ). For a component in tension, failure is assumed to happen when the maximum PEEQ reaches the critical value as given in Table 1. For shear connectors, the shear failure is defined as the PEEQ values reach the critical value of the bolt through the whole cross section. Similar approaches based on PEEQ were also adopted by other researches (Elflah *et al.* 2019a, Salih *et al.* 2010). The selected critical PEEQs in Table 1 are corresponding with the necking strain as obtained from the test stress-strain curves (Fig. 3). This strain value should be smaller than the actual fracture strain when the material breaks into two parts and will lead to conservative prediction of the rotation capacity. The reason of using necking strain instead of fracture strain is due to the fact that the material behavior beyond necking will be less predictable which involves strain localization and triaxial stress state. An explicit method to numerically simulate bolt failure should be based on certain damage or fracture models. This method is however far more complicated and such models are still not available for SS bolts.

2.2.2 Concrete

The nonlinear behaviour of concrete was modelled by the concrete damage plasticity model. The compressive strength was selected to be 25 MPa, while the tensile strength and elastic modulus are 2.5 MPa and 31000 MPa, respectively. The compressive stress-strain relationship of concrete was formularized by Mander's model (Mander *et al*. 1988) while the tensile stress was assumed to be linearly increased to the cracking strength and then dropped linearly to zero up to a maximum cracking strain of 0.002. The tensile stress-strain of concrete adopted in this study is a linear approximation of El-Tawil's model (El-Tawil and Deierlein 1996) for concrete with 25 MPa compressive strength.

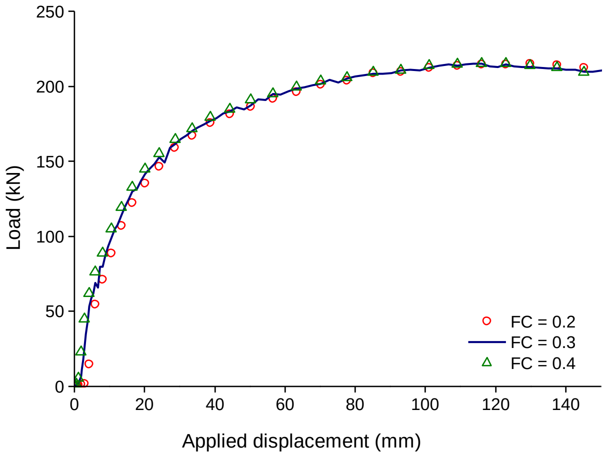

Fig. 5 Sensitivity to different friction coefficient (FC)

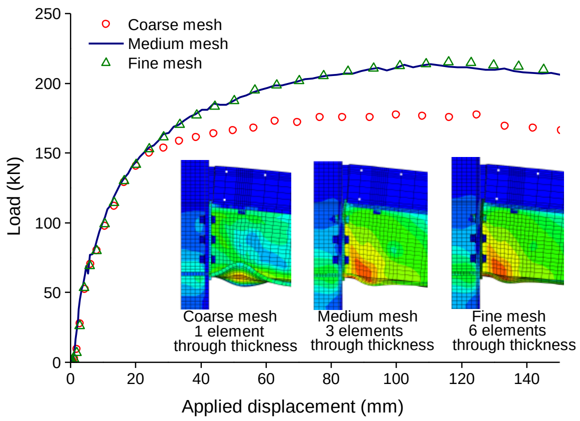

Fig. 6 Sensitivity to different mesh size

2.3 Sensitive analysis

In order to prevent the convergence issues encountered in an implicit solution algorithm (ABAQUS/Standard), the explicit dynamic solution module ABAQUS/Explicit was employed for the present FE model. As discussed in literature (Thai and Uy 2015, Song *et al*. 2016, Thai *et al*. 2017b), the "smooth step" amplitude of loading should be used corresponding with an effectively low loading speed to minimize the effects of inertial forces in a quasi-static analysis. A general accepted criterion is ensuring the ratio of kinetic-to-internal energy below 10% during the analysis (ABAQUS 2014). The effects of loading speed on the overall load-displacement response were investigated and discussed herein. Four levels of speed were trialed in the analysis ranging from 250 mm/s to 2000 mm/s, corresponding with the loading time of 0.5 s to 0.0625 s. The load-displacement curves obtained with different loading speeds are shown in Fig. 4(a). It can be observed that all curves except the one with the speed of 2000 mm/s are very close to each other, indicating a convergent trend when the speed is lower than 1000 mm/s. Furthermore, the applied load at the beam end and the reaction force at the column end are compared in Fig. 4(b) for different loading speeds, which is an alternative approach to examine whether an explicit dynamic analysis can be regarded as quasi-static. As can be seen, the curves of applied and reaction forces deviate largely at 2000 mm/s, indicating a significant dynamic effect. On the contrary, close match between applied and reaction forces can be observed at 500 mm/s and 250 mm/s. The ratio of kinetic-to-internal energy is also well below 10% during the analysis for these two cases. In this study, the loading speed of 250 mm/s was finally selected to ensure accurate results.

Besides the loading speed, the effects of friction coefficient and mesh size were also investigated in the sensitive analysis. As shown in Fig. 5, friction coefficients of 0.2, 0.3 (the one selected in the following analysis) and 0.4 were trialed, which indicates hardly any difference between the load-displacement curves. This is as expected as the bolted connections in the present joints are mainly in bearing type with very limit effects of friction. The effects of different mesh sizes are illustrated in Fig. 6, with 1, 3 or 6 elements through thickness in critical plates where large deflection or local bucking are expected to happen. It can be seen that the coarse mesh with only one layer of elements through thickness may be not sufficient to capture local bucking behaviour as the load-displacement curve deviate largely with the other two cases with medium and fine mesh. This is because the C3D8R element adopted in this study contains only one integration point therefore not able to simulate the distribution of bending stress through

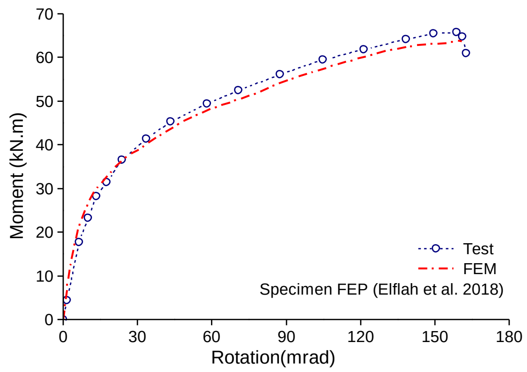

(a) Test vs. FEM moment-rotation responses

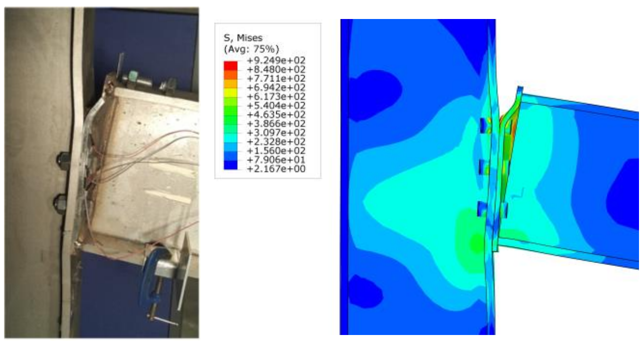

(b) Test vs. FEM failure modes (Elflah *et al*. 2019b)

Fig. 7 Model validation against SS joint with flush endplate connection (FEP)

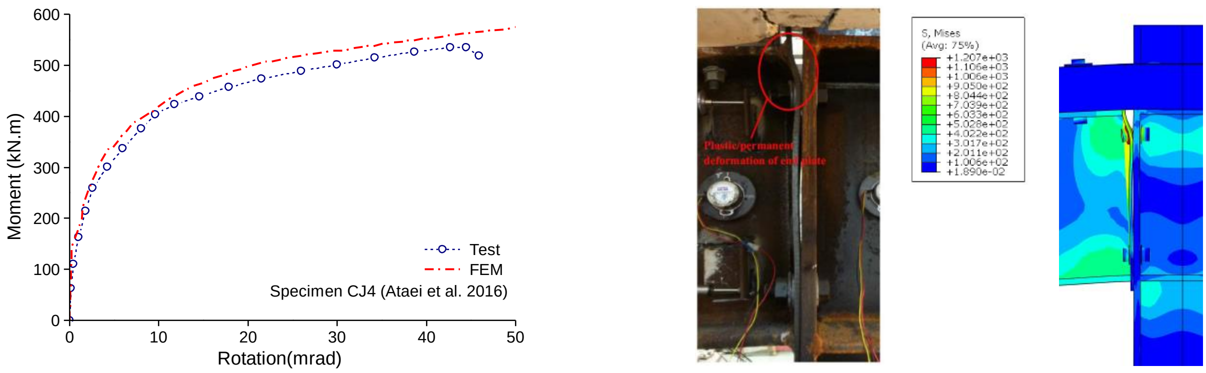

(a) Test vs. FEM moment-rotation responses (b) Test vs. FEM failure modes (Ataei *et al.* 2016)

Fig. 8 Model validation against CS composite joint with flush endplate connection (CJ4)

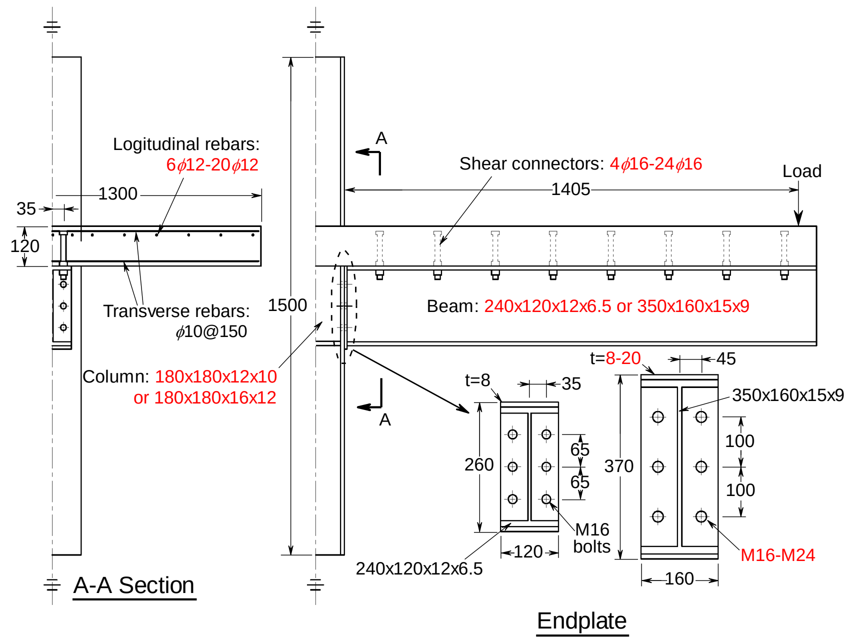

Fig. 9 Configuration of composite joint specimens

thickness with only one layer of elements. On the other hand, models with 3 (medium mesh) and 6 (fine mesh) layers of elements show convergence in terms of the load-displacement curve and consistency in predicting the bucking mode. In this study, the fine mesh with 6 elements through thickness was finally adopted since the computational time is generally acceptable.

2.4 Model validation

Since test data for SSCC joints are not available at present, the FE model was validated against monotonic loading tests of a pure SS joint, FEP (Elflah *et al.* 2019b) and a CS composite joint, CJ4 (Ataei *et al.* 2016), both involved flush endplate connections. Details of these test specimens are available in the original report and therefore not repeated herein. The same modelling technique and loading speed as described above were adopted for these specimens. Specially, pretension was applied to the bolted shear connectors of CJ4 by initial temperature changes of the bolt shank, as suggested by Thai and Uy (2015).

The moment-rotation responses and deformed shapes obtained from the FE analysis are compared with the test results of FEP and CJ4 in Figs. 7 and 8. Reasonable agreement can be observed between the test and FEM failure modes. The moment-rotation curves predicted by FEM are sufficiently close to the test results with -3.0% and +4.8% deviations of the moment corresponding to the ultimate rotation (rotation corresponding to the maximum moment from the test curves) for FEP and CJ4, respectively.

3. Parametric study

3.1 Description of selected parameters

Based on the validated FE model, a detailed parametric study was carried out, incorporating 45 joint specimens (29

Table 2 Selected parameters in the parametric analysis

Specimen	Material	Configuration*	Endplate thickness t_e 1.3 (mm)	Bolt diameter d (mm)	Beam dimension (mm)	Reinforcement (ρ)	Shear connectors (η)
SJ-SS-1	SS	**SJ, NS**	12	20	350×160×15×9	Nil	Nil
CJ-SS-1		**CJ, NS**				12Ø12 (1.03%)	16Ø16 (1.34)
CJ-SS-2		**CJ, BS**					
CJ-SS-3		**CJ, BTS**					
CJ-SS-4	SS	CJ, BS	**8**	20	350×160×15×9	12Ø12 (1.03%)	16Ø16 (1.34)
CJ-SS-5			**16**				
CJ-SS-6			**20**				
CJ-SS-7	SS	CJ, BS	12	**16**	350×160×15×9	12Ø12 (1.03%)	16Ø16 (1.34)
CJ-SS-8				**24**			
CJ-SS-9				**30**			
CJ-SS-10	SS	CJ, BS	12	20	350×160×15×9	**6Ø12 (0.51%)**	8Ø16 (1.34)
CJ-SS-11						**8Ø12 (0.69%)**	12Ø16 (1.51)
CJ-SS-12						**10Ø12 (0.86%)**	12Ø16 (1.21)
CJ-SS-13						**14Ø12 (1.20%)**	16Ø16 (1.15)
CJ-SS-14						**16Ø12 (1.37%)**	24Ø16 (1.51)
CJ-SS-15						**18Ø12 (1.54%)**	24Ø16 (1.34)
CJ-SS-16						**20Ø12 (1.71%)**	24Ø16 (1.21)
CJ-SS-17	SS	CJ, BS	8	16	240×120×12×6.5	**6Ø12 (0.51%)**	8Ø16 (1.34)
CJ-SS-18						**8Ø12 (0.69%)**	12Ø16 (1.51)
CJ-SS-19						**10Ø12 (0.86%)**	12Ø16 (1.21)
CJ-SS-20						**12Ø12 (1.03%)**	16Ø16 (1.34)
CJ-SS-21						**14Ø12 (1.20%)**	16Ø16 (1.15)
CJ-SS-22						**16Ø12 (1.37%)**	24Ø16 (1.51)
CJ-SS-23						**18Ø12 (1.54%)**	24Ø16 (1.34)
CJ-SS-24						**20Ø12 (1.71%)**	24Ø16 (1.21)
CJ-SS-25	SS	CJ, BS	8	16	240×120×12×6.5	12Ø12 (1.03%)	**4Ø16 (0.34)**
CJ-SS-26							**6Ø16 (0.50)**
CJ-SS-27							**8Ø16 (0.67)**
CJ-SS-28							**12Ø16 (1.01)**
CJ-CS-1	**CS**	CJ, BS	12	20	350×160×15×9	**6Ø12 (0.51%)**	8Ø16 (1.23)
CJ-CS-2						**8Ø12 (0.69%)**	12Ø16 (1.39)
CJ-CS-3						**10Ø12 (0.86%)**	12Ø16 (1.11)
CJ-CS-4						**12Ø12 (1.03%)**	16Ø16 (1.23)
CJ-CS-5						**14Ø12 (1.20%)**	16Ø16 (1.06)
CJ-CS-6						**16Ø12 (1.37%)**	24Ø16 (1.39)
CJ-CS-7						**18Ø12 (1.54%)**	24Ø16 (1.23)
CJ-CS-8						**20Ø12 (1.71%)**	24Ø16 (1.11)
CJ-CS-9	**CS**	CJ, BS	8	16	240×120×12×6.5	**6Ø12 (0.51%)**	8Ø16 (1.23)
CJ-CS-10						**8Ø12 (0.69%)**	12Ø16 (1.39)
CJ-CS-11						**10Ø12 (0.86%)**	12Ø16 (1.11)
CJ-CS-12						**12Ø12 (1.03%)**	16Ø16 (1.23)
CJ-CS-13						**14Ø12 (1.20%)**	16Ø16 (1.06)
CJ-CS-14						**16Ø12 (1.37%)**	24Ø16 (1.39)
CJ-CS-15						**18Ø12 (1.54%)**	24Ø16 (1.23)
CJ-CS-16						**20Ø12 (1.71%)**	24Ø16 (1.11)

*SJ = Steel joint, CJ = Composite joint, NS = No column web stiffener, BS = Bottom stiffener for column web in compression, BTS = Bottom and top stiffeners for column web in compression and tension

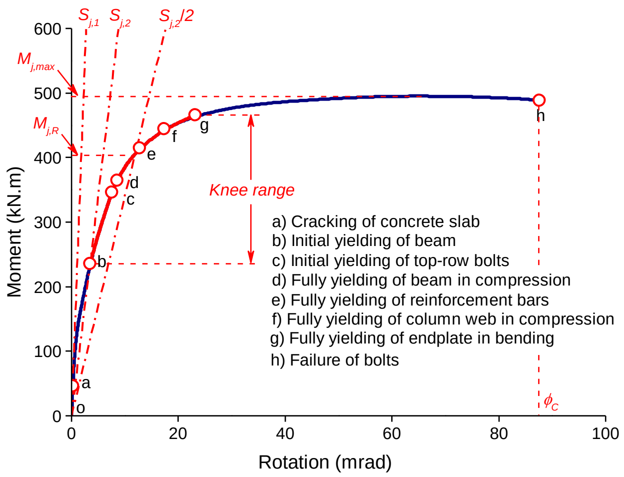

Fig. 10 Typical moment-rotation response of a SSCC joint from FE analysis

SS and 16 CS). Details of the joint configuration are shown in Fig. 9. Two sets of beam/column sizes (beam: 350 × 160 × 15 × 9 mm or 240 × 120 × 12 × 6.5 mm; column: 180 × 180 × 16 × 12 mm or 180 × 180 × 12 × 10 mm) were selected in order to cover common engineering applications. The selected beam/column sections can be classified as Class 1 or compact sections as specified in Eurocode for SS structures (CEN 2015). The concrete slab is 120 mm deep with an effective width of 1300 mm, which is around seven times the column depth as suggested by Leon and Zandonini (1992) and Liew *et al.* (2000). The considered parameters include material of steel, joint configuration, endplate thickness t_e, bolt diameter d, reinforcement ratio ρ, and shear connection degree η. Parameters of the specimens are summarized in Table 2. As previously described, the compressive strength of concrete was selected as 25 MPa in all the cases, which was determined based on the resistance of the bolted shear connectors in accordance with AS/NZS 2327 (AS/NZS 2017), i.e. by ensuring similar resistances of a single shear connector in shear and the concrete slab in bearing. Full shear connection ($\eta \geq 1$) was ensured for all composite specimens except CJ-SS-25, 26 and 27, which were designed to investigate the effects of partial shear connection.

3.2 Characterization of moment-rotation responses

The flexural behaviour of a beam-to-column joint is characterized by its moment-rotation response. The moment can be calculated multiplying the lever arm length (1405 mm in this study) by the recorded forces at the beam end. The rotation of the joint was obtained through an indirect approach, i.e., dividing the difference between the displacements (along the direction of the beam axis) measured at the beam top and bottom flanges by the depth of the beam. Fig. 10 shows a typical moment-rotation curve of a SSCC joint, on which several critical states (point a-h) can be identified. Sudden change of stiffness can be observed as cracking initiates in the concrete slab (point a), followed by constant increase in moment capacity and decrease in rotational stiffness corresponding with gradual yielding of the steel components (known as knee range b-g). The moment capacity is still able to increase slightly after complete yielding of the joint (point g), which is due to strain hardening of the steel components. From the moment-rotation response, three main properties need to be defined: the initial stiffness $S_{j,ini}$, the plastic moment resistance (abbreviated as the moment resistance) $M_{j,R}$, and the rotation capacity ϕ_C.

An exact initial stiffness of a composite joint should be determined by linear regression of the initial moment-rotation response prior to tensile cracking (o-a in Fig. 10). This stiffness (referred to as the first stiffness $S_{j,1}$ in this study) however, may be less meaningful from a practical point of view, as it is difficult to be accurately measured through actual experimental tests due to early cracking of the concrete slab. The contribution of uncracked concrete to the initial stiffness of composite joints is also neglected by existing design methods (as discussed in Section 4.1). Therefore, a second stiffness $S_{j,2}$ was defined in this study, which is the secant stiffness between the origin o and the point b where yielding initiates in the steel components. The second stiffness can be used to represent the pre-yield stiffness of a composite joint without the contribution of uncracked concrete.

Although the (plastic) moment resistance is perhaps the most important property of a composite beam-to-column joint for designers, it is still not clear how it can be determined from an experimental or numerical moment-rotation curve. For steel joints, several methods were adopted in previous studies, among which the most commonly used one (Girão Coelho and Bijlaard 2007, Wang *et al.* 2018b, Elflah *et al.* 2019b, Li *et al.* 2019b) defines the moment resistance as corresponds to the intersection between the tangent to the initial elastic part (or the ordinate) and the tangent to the post-yielding hardening part of the moment-rotation curve. Although this method works well for steel joints with typical elastic-plastic and near-linear hardening behaviour, it seems less appropriate for composite joints. Different from steel joints, the stiffness of the hardening portion (g-h in Fig. 10) of a composite joint changes significantly due to the complex load-carrying mechanism and the occurrence of local buckling in the compression zone. The determination of

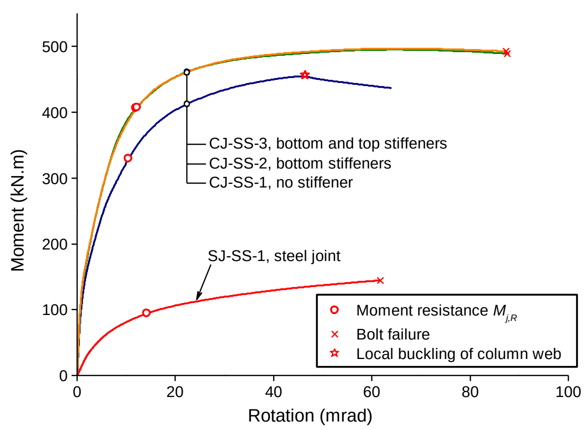

Fig. 11 Moment-rotation curves of joints with different configurations

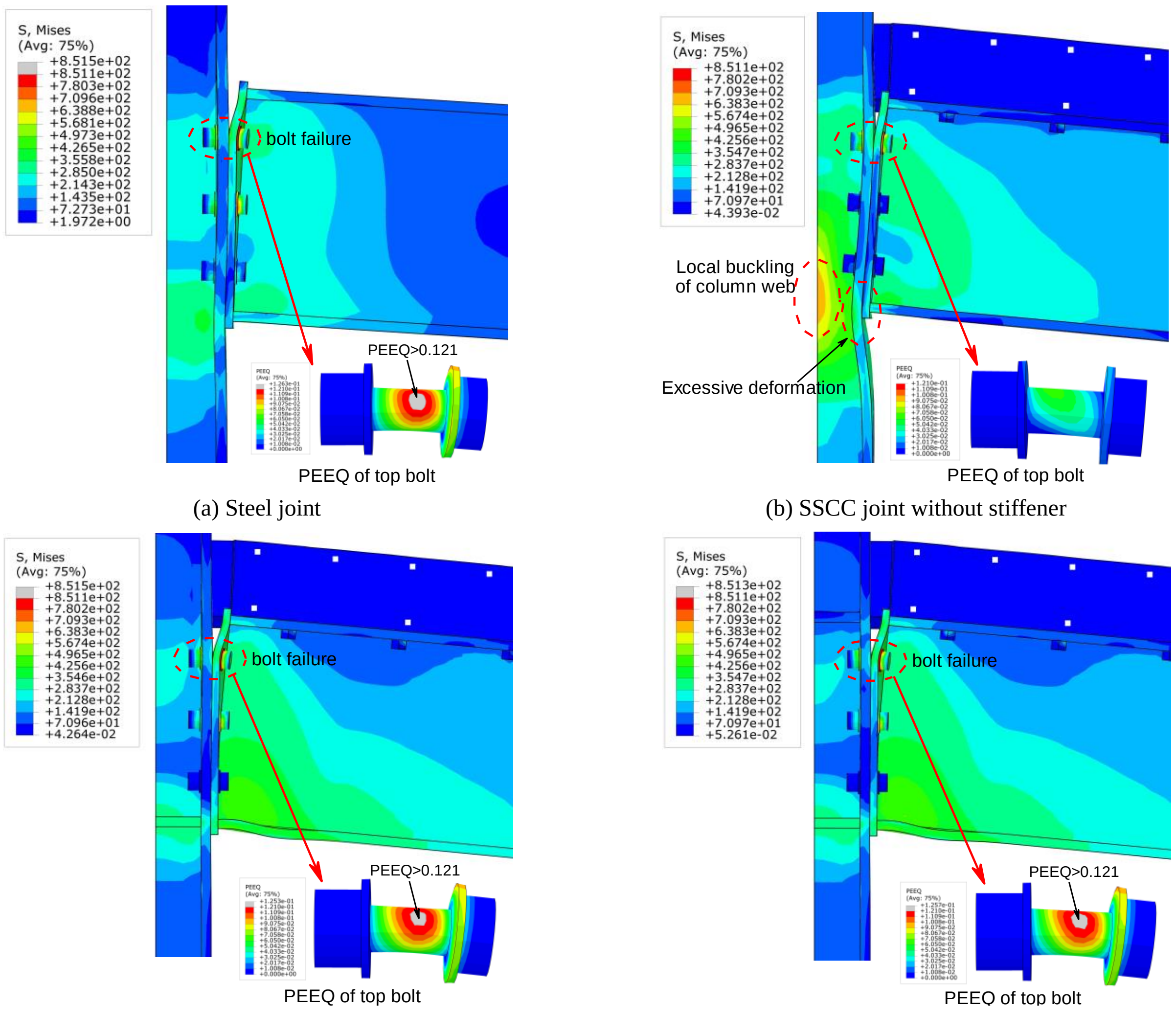

(a) Steel joint

(b) SSCC joint without stiffener

(c) SSCC joint with bottom stiffeners

(d) SSCC joint with top and bottom stiffeners

Fig. 12 Failure modes of joints with different configurations

an appropriate "hardening" stiffness is thus difficult and highly subjective. For these reasons, an alternative approach is adopted in this study as illustrated in Fig. 10. The moment resistance is defined as corresponding to a secant of one-half the second stiffness $S_{j,2}$ on the moment rotation curve. This method was proved to give reasonable yet objective estimations of the moment resistance $M_{j,R}$ for both SS and CS composite joints.

The rotation capacity of a joint is the maximum rotation it can reach without significant drop in the moment, always

Table 3 Measured properties and design predictions of SS and CS composite joints

Specimen	Failure mode*	Initial stiffness (kN.m/mrad)					Plastic moment resistance (kN.m)					Maximum moment $M_{j,max}$ (kN.m)	Rotation capacity ϕ_C (mrad)
		FEM $S_{j,1,fem}$	FEM $S_{j,2,fem}$	Design $S_{j,ini,d}$	$S_{j,ini,d}/S_{j,1,fem}$	$S_{j,ini,d}/S_{j,2,fem}$	FEM $M_{j,R,fem}$	EC3/4 $M_{j,R,ec}$	AS/NZS 2327 $M_{j,R,as}$	$M_{j,R,ec}/M_{j,R,fem}$	$M_{j,R,as}/M_{j,R,fem}$		
SJ-SS-1	B	16.0	13.4				94.4					144.4	61.8
CJ-SS-1	E	166.6	63.4	89.4	**0.537**	**1.410**	330.0	262.6	262.6	**0.796**	**0.796**	456.2	46.4
CJ-SS-2	B	221.3	68.1	144.7	**0.654**	**2.125**	406.6	391.4	302.3	**0.963**	**0.743**	496.1	87.6
CJ-SS-3	B	221.7	67.0	168.7	**0.761**	**2.518**	407.8	391.4	302.3	**0.960**	**0.741**	502.4	87.4
CJ-SS-4	A	220.3	66.4	124.6	**0.566**	**1.877**	387.2	371.0	308.4	**0.958**	**0.796**	466.1	100.4
CJ-SS-5	B	223.2	67.7	154.1	**0.690**	**2.276**	413.2	391.4	298.2	**0.947**	**0.722**	514.7	68.3
CJ-SS-6	B	225.4	68.4	157.6	**0.699**	**2.304**	418.5	391.4	294.9	**0.935**	**0.705**	520.6	65.7

*A: Failure of reinforcing bars; B: Failure of top-row bolts; C: Failure of shear connection; D: Local buckling of beam flange/web; E: Local buckling of column web

Table 3 Continued

Specimen	Failure mode*	Initial stiffness (kN.m/mrad)					Plastic moment resistance (kN.m)					Maximum moment $M_{j,max}$ (kN.m)	Rotation capacity ϕ_C (mrad)
		FEM $S_{j,1,fem}$	FEM $S_{j,2,fem}$	Design $S_{j,ini,d}$	$S_{j,ini,d}/S_{j,1,fem}$	$S_{j,ini,d}/S_{j,2,fem}$	FEM $M_{j,R,fem}$	EC3/4 $M_{j,R,ec}$	AS/NZS 2327 $M_{j,R,as}$	$M_{j,R,ec}/M_{j,R,fem}$	$M_{j,R,as}/M_{j,R,fem}$		
CJ-SS-7	B	222.6	65.8	140.5	**0.631**	**2.135**	406.7	379.4	305.9	**0.933**	**0.752**	485.5	54.8
CJ-SS-8	B	222.0	68.7	147.1	**0.663**	**2.141**	405.8	391.4	302.3	**0.965**	**0.745**	519.7	104.1
CJ-SS-9	A	220.8	71.3	149.9	**0.679**	**2.102**	406.1	391.4	302.3	**0.964**	**0.744**	535.2	119.0
CJ-SS-10	B	160.9	45.6	90.2	**0.561**	**1.978**	286.3	226.0	226.0	**0.789**	**0.789**	340.0	65.4
CJ-SS-11	B	194.5	55.4	110.7	**0.569**	**1.998**	328.2	281.5	281.5	**0.858**	**0.858**	392.7	69.6
CJ-SS-12	B	195.1	61.7	120.7	**0.619**	**1.956**	367.5	337.0	337.0	**0.917**	**0.917**	447.0	79.0
CJ-SS-13	B	222.8	73.5	155.7	**0.699**	**2.118**	433.8	406.3	304.6	**0.937**	**0.702**	546.4	98.0
CJ-SS-14	B	248.8	79.4	199.1	**0.800**	**2.508**	456.8	408.7	306.5	**0.889**	**0.667**	591.9	108.7
CJ-SS-15	D	250.3	80.0	214.0	**0.855**	**2.675**	485.3	410.6	307.9	**0.846**	**0.634**	640.8	108.0
CJ-SS-16	D	251.1	85.5	228.5	**0.910**	**2.673**	499.0	412.2	309.1	**0.826**	**0.619**	665.0	68.6
CJ-SS-17	B	85.3	29.7	41.7	**0.489**	**1.404**	156.3	144.2	144.2	**0.923**	**0.923**	213.0	130.2
CJ-SS-18	B	99.3	34.1	58.0	**0.584**	**1.701**	185.9	176.5	142.4	**0.949**	**0.766**	254.6	161.3
CJ-SS-19	D	99.6	37.7	66.7	**0.670**	**1.769**	204.8	177.9	143.5	**0.869**	**0.701**	286.3	169.6
CJ-SS-20	D	112.4	41.3	88.8	**0.790**	**2.150**	219.3	178.8	144.2	**0.815**	**0.657**	308.1	79.5
CJ-SS-21	D	114.2	44.4	100.0	**0.876**	**2.252**	227.2	179.5	144.8	**0.790**	**0.637**	314.3	51.8
CJ-SS-22	D	125.9	47.2	146.8	**1.166**	**3.110**	242.2	180.0	145.2	**0.743**	**0.600**	321.8	44.1
CJ-SS-23	D	125.9	50.1	166.1	**1.319**	**3.315**	245.6	180.4	145.6	**0.735**	**0.593**	330.9	39.4
CJ-SS-24	D	126.5	49.4	186.4	**1.474**	**3.773**	256.5	180.8	145.8	**0.705**	**0.569**	336.8	38.4
CJ-SS-25	C	60.0	25.6				183.2					223.0	31.7
CJ-SS-26	C	77.4	34.7				200.5					284.2	52.7
CJ-SS-27	C	88.9	37.9				211.3					305.0	68.6
CJ-SS-28	D	100.7	41.4				211.4					306.9	72.4
AVG. (SS)					**0.761**	**2.261**				**0.876**	**0.724**		
SDV. (SS)					**0.240**	**0.544**				**0.081**	**0.093**		
CJ-CS-1	B	163.8	60.2	90.2	**0.551**	**1.498**	328.4	262.6	262.6	**0.800**	**0.800**	402.3	33.8
CJ-CS-2	B	197.1	67.2	110.7	**0.562**	**1.647**	380.9	322.8	322.8	**0.847**	**0.847**	467.4	37.9
CJ-CS-3	B	198.3	74.0	120.7	**0.609**	**1.631**	427.3	383.0	383.0	**0.896**	**0.896**	531.0	41.9
CJ-CS-4	B	226.4	82.2	144.7	**0.639**	**1.760**	474.6	443.3	443.3	**0.934**	**0.934**	586.8	46.8
CJ-CS-5	B	223.4	86.8	155.7	**0.697**	**1.794**	502.0	503.5	414.0	**1.003**	**0.825**	646.4	52.1
CJ-CS-6	B	247.3	92.2	199.1	**0.805**	**2.159**	542.0	547.6	417.0	**1.010**	**0.769**	707.6	57.5
CJ-CS-7	B	251.7	92.4	214.0	**0.850**	**2.316**	576.5	559.3	419.4	**0.970**	**0.727**	743.7	63.8
CJ-CS-8	B	253.1	97.3	228.5	**0.903**	**2.348**	592.7	561.9	421.4	**0.948**	**0.711**	796.1	74.3
CJ-CS-9	B	86.3	31.3	41.7	**0.483**	**1.332**	185.5	161.2	161.2	**0.869**	**0.869**	241.9	56.4
CJ-CS-10	B	100.6	35.7	58.0	**0.577**	**1.625**	220.6	207.6	207.6	**0.941**	**0.941**	290.8	67.5
CJ-CS-11	B	99.4	41.3	66.7	**0.671**	**1.615**	241.1	242.7	195.8	**1.007**	**0.812**	334.3	82.7
CJ-CS-12	B	109.6	46.4	88.8	**0.810**	**1.914**	251.7	244.3	197.1	**0.971**	**0.783**	371.0	102.7
CJ-CS-13	B	110.4	49.1	100.0	**0.906**	**2.037**	264.3	245.4	198.0	**0.928**	**0.749**	397.8	136.0
CJ-CS-14	D	119.0	53.5	146.8	**1.234**	**2.744**	273.5	246.3	198.7	**0.901**	**0.726**	413.4	92.8
CJ-CS-15	D	119.0	57.3	166.1	**1.396**	**2.899**	278.5	247.0	199.3	**0.887**	**0.716**	425.7	80.0
CJ-CS-16	D	119.5	58.2	186.4	**1.560**	**3.203**	287.2	247.6	199.7	**0.862**	**0.695**	449.0	73.9
AVG. (CS)					**0.828**	**2.033**				**0.923**	**0.800**		
SDV. (CS)					**0.305**	**0.524**				**0.060**	**0.077**		

*A: Failure of reinforcing bars; B: Failure of top-row bolts; C: Failure of shear connection; D: Local buckling of beam flange/web; E: Local buckling of column web corresponding with final failure of the joint. From the observations of the FE results, five failure modes are identified that determine the rotation capacity:

A) Failure of reinforcing bars.
B) Failure of top-row bolts.
C) Failure of shear connection.
D) Local buckling of beam flange/web.
E) Local buckling of column web.

A summary of the key properties and failure modes obtained from the parametric study is given in Table 3. The effects of each parameter on the moment-rotation response are discussed in the following sections.

3.3 Effects of joint configuration

Four different joint configurations were considered in the parametric study, including a pure steel joint (SJ-SS-1), and composite joints with different types of stiffeners at the column web panel: i.e., without stiffener (CJ-SS-1), bottom stiffeners at compression zone (CJ-SS-2) and bottom and top stiffeners at both compression and tension zones (CJ-SS-3).

The computed moment-rotation curves for different joint configurations are shown in Fig. 11, while the resultant failure modes are displayed in Fig. 12. It is obvious that by introducing composite action to SS joints, significant enhancement can be achieved in both initial stiffness and moment resistance. It can be seen from Table 3 that the second stiffness of CJ-SS-2 is around five times that of SJ-SS-1; while the increase in the moment resistance is around four times.

Regarding different stiffening configurations for SSCC joints, it can be found that joints with column web stiffeners have higher initial stiffness, moment resistance and rotation capacity than the one without stiffener. Different from the stiffened joints which are failed at the top bolts, the failure mode of the unstiffened joint is dominated by local buckling of the column web panel, corresponding with excessive bending deformation of the column flange (Fig. 12(b)). At the meantime, the strains (PEEQ) in the top bolts are still very low, indicating that the strength is not sufficiently developed in the tension zone. A comparison between CJ-SS-2 and CJ-SS-3 reveals that the top stiffener has actually no contribution to strengthening the joint. This is as expected because the stresses of the column web/flange for CJ-SS-2 are very low at the level of the top stiffener. Therefore, it may be concluded that the top stiffeners are not necessary for SSCC joints under symmetric hogging moments.

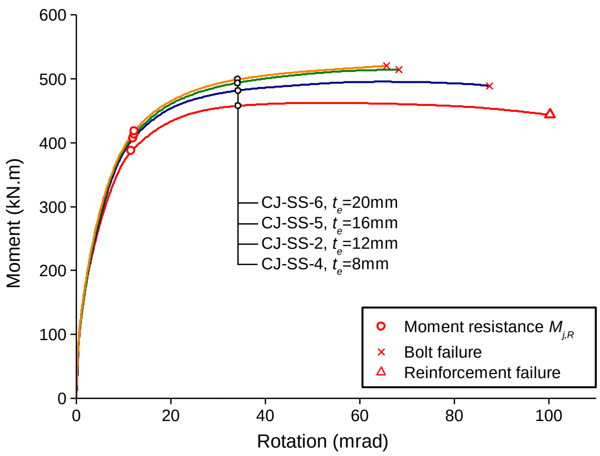

Fig. 13 Moment-rotation curves of SSCC joints with different endplate thickness

3.4 Effects of endplate thickness

The moment-rotation curves of SSCC joints with different endplate thickness (8 mm-20 mm) are shown in Fig. 13. Failure modes of the equivalent T-stubs (representing the endplates in bending) of different specimens are compared in Fig. 14. It can be seen that the moment resistance and the initial stiffness are only slightly enhanced with the increase of the endplate thickness from 8 to 20 mm. For the specimen with 8mm thick endplate (CJ-SS-4),

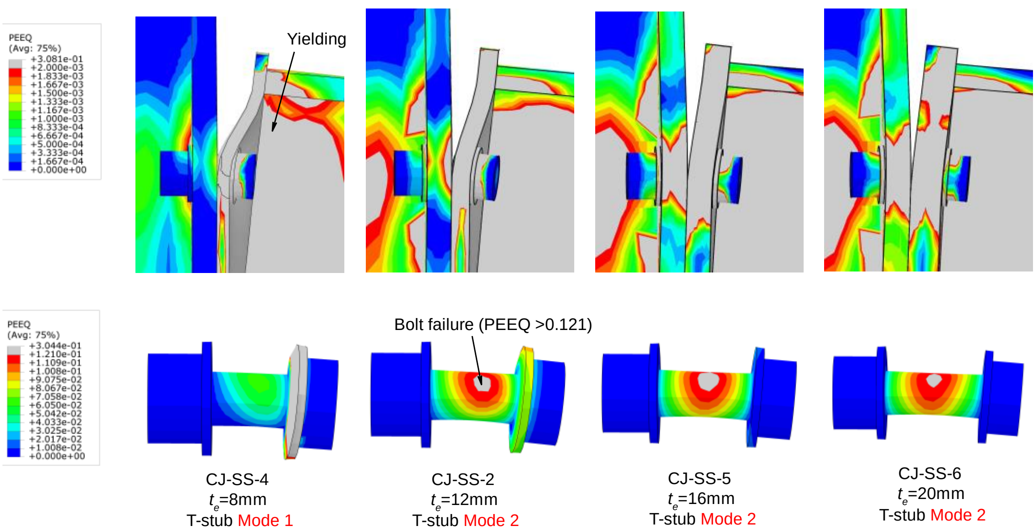

Fig. 14 Failure modes of SSCC joints with different endplate thickness

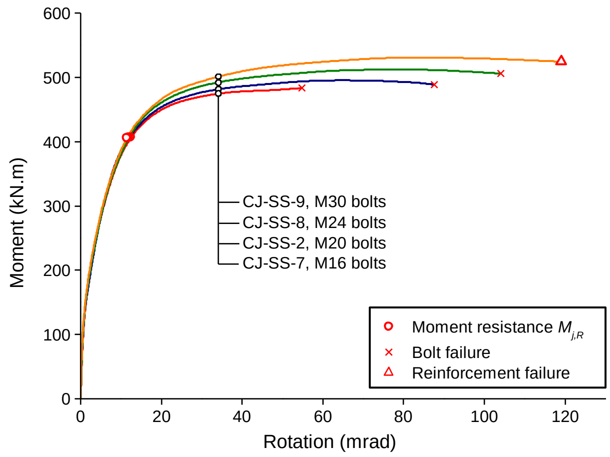

Fig. 15 Moment-rotation curves of SSCC joints with different bolt diameters

the column flange does not yield at failure, indicating that the moment capacity is still able to increase by increasing the endplate thickness. Although excessive plastic deformation is observed at the endplate, failure does not occur in the bolt shank. Therefore, the equivalent T-stub of the endplate can be classified as mode 1, i.e., yielding of the T-stub flange without bolt failure. Since the final failure of the joint is triggered by failure of the reinforcements for this specimen, the rotation capacity is higher than all the other cases. For joints with thicker endplates (12-20 mm), the equivalent T-stubs fail by mode 2, i.e., bolt failure with yielding of the flange. In these cases, increasing the endplate thickness leads to earlier failure of bolts and thus a decrease in the rotation capacity. Therefore, it is suggested to limit the thickness of the endplate (for the present configuration no more than 12 mm) for SSCC joints from a practical point of view.

3.5 Effects of bolt diameter

Fig. 15 shows the moment-rotation curves of SSCC joints with different bolt diameters from M16 to M30. Similar to the cases for different endplate thickness, the bolt diameter does not have notable influence on the moment resistance nor on the initial stiffness of the joint. As the bolt diameter increases, the equivalent T-stub of the endplate changes from mode 2 (M16-M24) to mode 1(M30), corresponding with an increase in the rotation capacity.

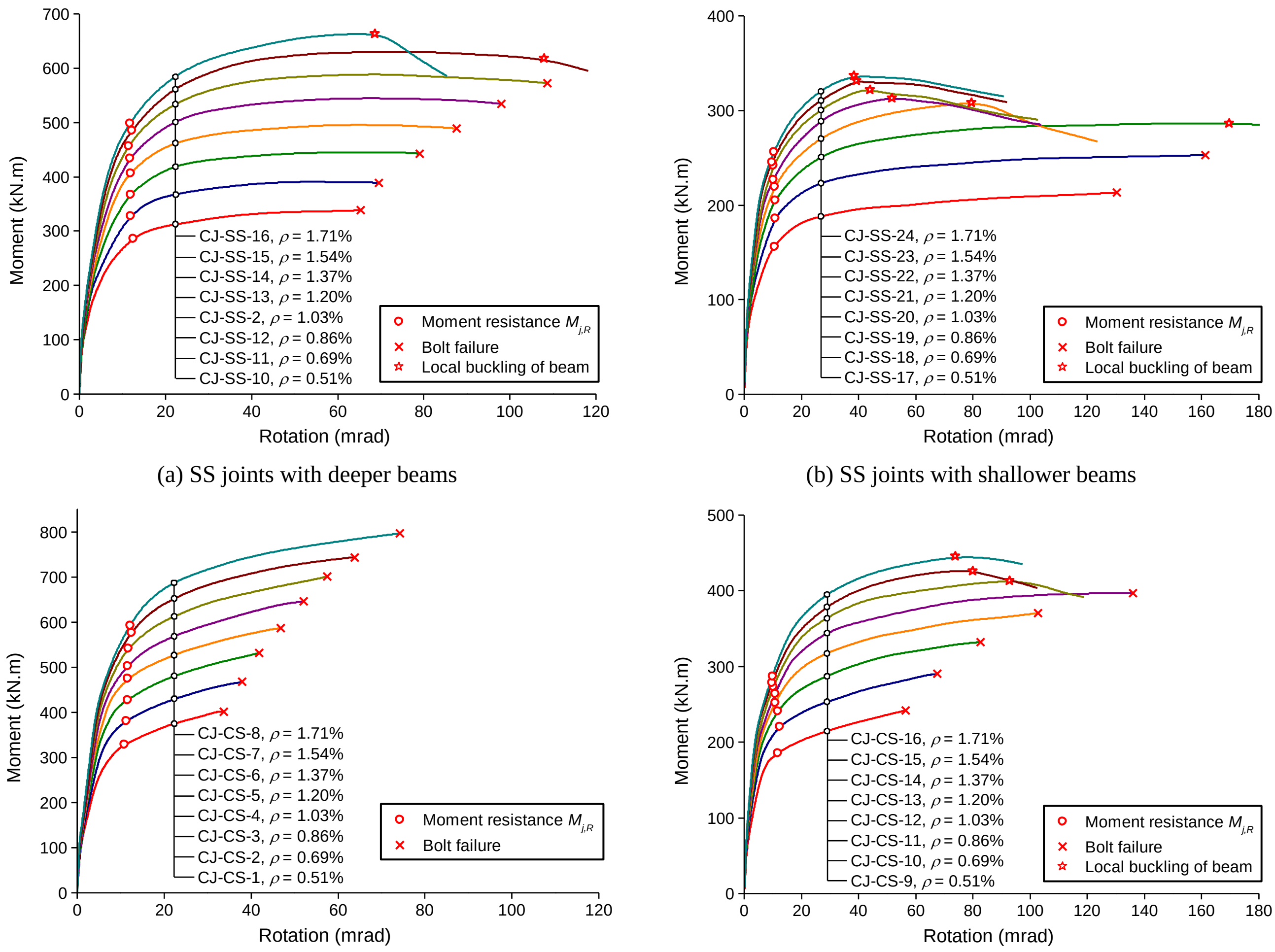

(a) SS joints with deeper beams (b) SS joints with shallower beams

(c) CS joints with deeper beams (d) CS joints with shallower beams

Fig. 16 Moment-rotation curves of composite joints with different reinforcement ratios

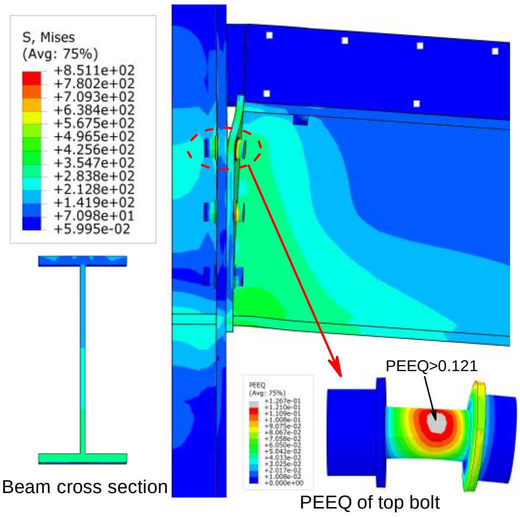

(a) Deeper beams with low reinforcement ratio

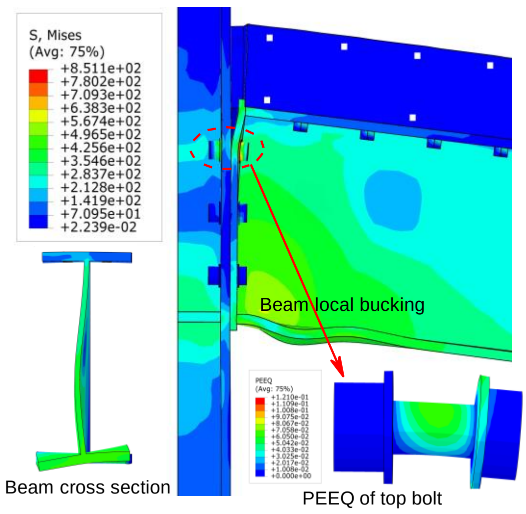

(b) Deeper beams with high reinforcement ratio

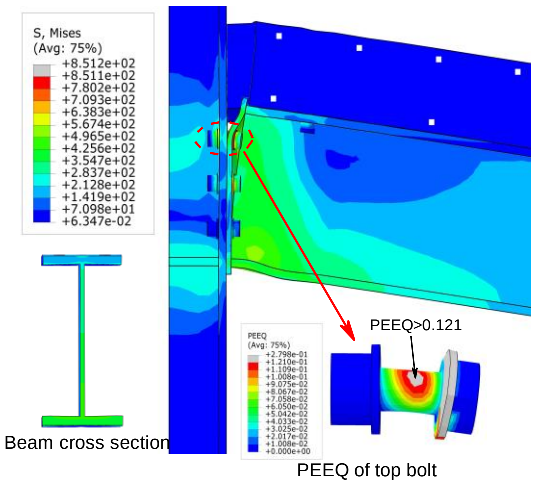

(c) Shallower beams with low reinforcement ratio

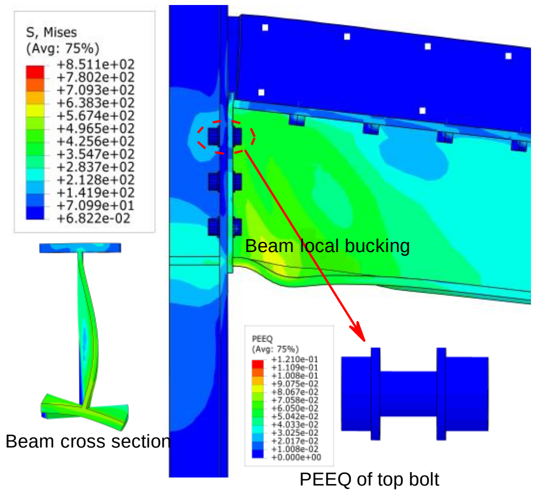

(d) Shallower beams with high reinforcement ratio

Fig. 17 Failure modes of SSCC joints with different reinforcement ratios

3.6 Effects of reinforcement ratio

It was confirmed in a number of studies (Xiao *et al*. 1994, Liew *et al*. 2000, Loh *et al*. 2006b, Thai and Uy 2015) that the reinforcement ratio is a key factor that significantly affects the moment-rotation response of composite joints. In this study, specimens with a wide rangeof reinforcement ratio from 0.51% to 1.71% were analysed, which include composite joints with deeper (350×160×15× 9 mm) or shallower (240×120×12×6.5 mm) steel beams. For these specimens, the number of shear connectors was increased correspondingly with the increase of the reinforcement ratio to ensure full shear connection. Both CS and SS composite joints were incorporated in the analysis for comparisons.

Moment-rotation curves and failure modes for SS and CS composite joints with deeper or shallower beams are shown in Figs. 16 and 17, respectively. The effects of the reinforcement ratio on individual properties ($S_{j,1}$, $S_{j,2}$, $M_{j,R}$, and ϕ_C) are illustrated in Fig. 18. At relatively low reinforcement ratios, failure of the joint is dominated by bolt failure, i.e., the maximum PEEQ in the bolt shank reaches the critical value (Figs. 17 (a) and (c)). This is due to the fact that the SS/CS bolts are the most brittle components within a joint as shown in Fig. 3. In these cases the initial stiffness (refers to either first or second stiffness), the moment resistance and the rotation capacity of the joints increase monotonically with the increase of the reinforcement ratio. When the reinforcement ratio reaches a certain level, the failure mode changes from bolt failure to local bucking of beam flange/web in the compression zone (Figs. 17(b) and (d)). In order to identify the occurrence of local bucking, a method based on the measurement of local surface strain was utilized as described by Song *et al*. (2019) and Li *et al*. (2019). For these cases, the rotation capacity decreases with the increased reinforcement ratio due to earlier local buckling of the compression zone of the beam. On the other hand, the initial stiffness and the moment resistance still increase as the reinforcement ratio increases.

It can be further noticed from Fig. 18 that composite joints with deeper beams possess higher moment resistance

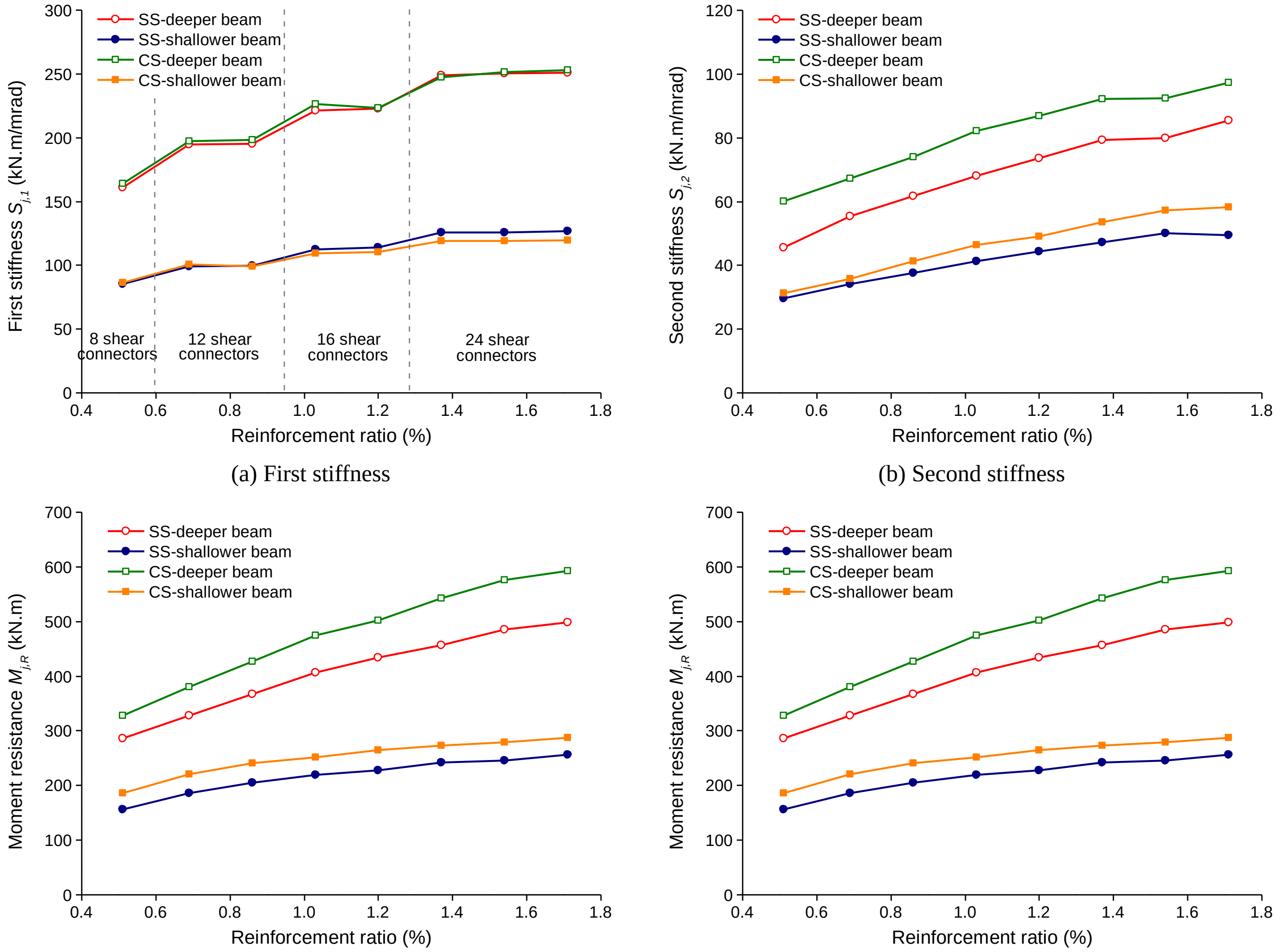

(a) First stiffness

(b) Second stiffness

(c) Moment resistance

(d) Rotation capacity

Fig. 18 Effects of reinforcement ratio on key properties of SSCC joints

and initial stiffness than those with shallower beams. This is as expected due to larger lever arms of the tension components (bolts and reinforcement) and also stronger compression zone of the beam. The first stiffness of CS and SS joints are very similar with the same reinforcement ratio and beam size due to similar elastic modulus of CS and SS components. Actually, the first stiffness seems to be related to the number of shear connectors, not the reinforcement ratio, as shown in Fig. 18(a). The second stiffness of CS joints is slightly higher than that of SS joints as can be found from Fig. 18(b), which may be attributed to the rounded stress-strain curve of stainless steel and generally larger yielding strain compared with carbon steel. Furthermore, CS joints also have higher moment resistance than SS joints due to higher yield stress of CS components. As shown in Fig. 18(c), the rotation capacity of SS joints is significantly higher than that of CS joints if failure of the joint is triggered by bolt failure, since SS bolts are much more ductile than CS counterparts. However, it is also observed that SS beams are obviously more susceptible to local bucking than CS beams, which leads to lower rotation capacity of SS joints than CS ones at high reinforcement ratios.

3.7 Effects of degree of shear connection

The effects of shear connection degree on the moment-rotation behaviour of SSCC joints are illustrated in Fig. 19. For joints with full shear connection ($\eta > 1$), the degree of shear connection does not have significant influence on the moment-rotation response, in terms of the initial stiffness, the moment resistance and the rotation capacity. For joints with partial shear connection, however, by reducing the degree of shear connection, both the moment resistance and the initial stiffness will decrease considerably. The rotation capacity will decrease significantly with reduced shear connection degree as the failure of the joint is triggered by failure of the shear connectors rather than local bucking of the beam.

4. Appraisal of design methods

In this chapter, comparisons are made between the FEM results and the predicted values by the present codes of practice (CEN 2004, AS/NZS 2017) regarding initial stiffness, moment resistance, and moment-rotation characteristic of composite joints. Note that there is still no

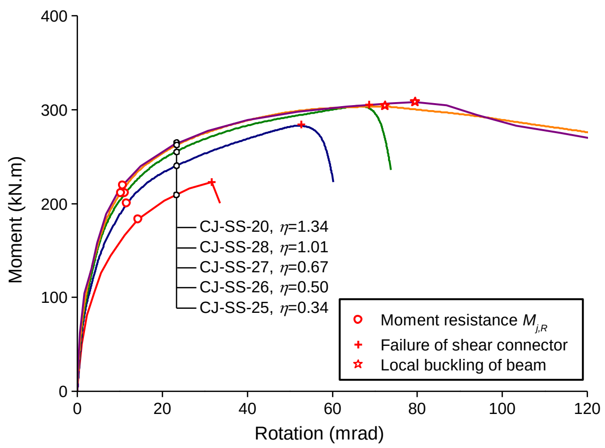

Fig. 19 Moment-rotation curves of SSCC joints with different shear connection degrees

systematic framework in design codes for quantitatively evaluating the rotation capacity of composite joints failed by bolt/reinforcement failure or local buckling of beam. Therefore, the design method regarding rotation capacity will not be discussed herein. It should be noted that the method in Eurocode 4 (EC4) is basically borrowed from EC3 (CEN 2005) with modifications considering the characteristics of composite joints. Therefore, the Eurocode method is referred to as EC3/4 in the following discussions.

4.1 Initial stiffness

The calculation methods in EC3/4 and AS/NZS 2327 regarding the initial stiffness are essentially the same, which are based on the "component method", i.e., determining the stiffness of a joint from the stiffness contributions of its basic components. Concerning a composite joint with flush endplate under symmetric hogging moments, the basic stiffness components include: (1) column web in compression k_2; (2) column web in tension k_3; (3) column flange in bending k_4; (4) endplate in bending k_5; (5) Bolts in tension k_{10}; (6) reinforcements in tension $k_{s,r}$. For the joint configuration in this study with three rows of bolts, it was found that the contributions of the second and third bolt rows to the initial stiffness and the moment resistance are negligible and therefore omitted in the calculation. The initial stiffness of the joint is thus calculated as

$$S_{j,ini,d} = \frac{E {z_{eq}}^2}{\frac{1}{k_2} + \frac{1}{k_{eq}}} \tag{1}$$

where E is the elastic modulus of steel, k_{eq} is the equivalent stiffness coefficient of the tension zone (including the reinforcement and the first bolt row)

$$k_{eq} = \frac{k_{eff,b} z_b + k_{s,r} z_r}{z_{eq}} \tag{2}$$

where z_b and z_r are the distances from the first bolt row or the reinforcement to the centre of the compression flange. $k_{eff,b}$ is the effective stiffness coefficient of the first bow row

$$k_{eff,b} = \frac{1}{\frac{1}{k_3} + \frac{1}{k_4} + \frac{1}{k_5} + \frac{1}{k_{10}}} \tag{3}$$

z_{eq} is the equivalent lever arm of the tension zone

$$z_{eq} = \frac{k_{eff,b} {z_b}^2 + k_{s,r} {z_r}^2}{k_{eff,b} z_b + k_{s,r} z_r} \tag{4}$$

The stiffness coefficients for different components can be calculated according to the design codes. Specifically, the coefficient for reinforcement $k_{s,r}$ has taken into account the effects of shear connection, which is related to the stiffness of a single shear connector k_{sc}, corresponding to 0.7 times the resistance of the shear connector. The suggested value for k_{sc} of a 19 mm diameter headed stud is 100 kN/mm in the design codes. For bolted shear connectors however, there is no suggested value. Based on push-out test results, Pavlovic *et al*. (2013) proposed that k_{sc} is equal to 68 kN/mm for a M16 bolted shear connector. This value was adopted in this study to calculate the initial stiffness of the joints.

The initial stiffness values predicted by the design codes were compared with the first and second stiffness measured from the numerical analysis, as shown in Table 3 and Fig. 20. It can be seen that the predictions of the design codes are generally conservative compared with the measured first stiffness $S_{j,1,fem}$ of composite joints. The average design to FEM ratios $S_{j,ini,d}/S_{j,1,fem}$ are 0.761 and 0.828 respectively for SS and CS joints. This may be due to the fact that the design method does not take into account the stiffness contribution of uncracked concrete. On the other hand, the

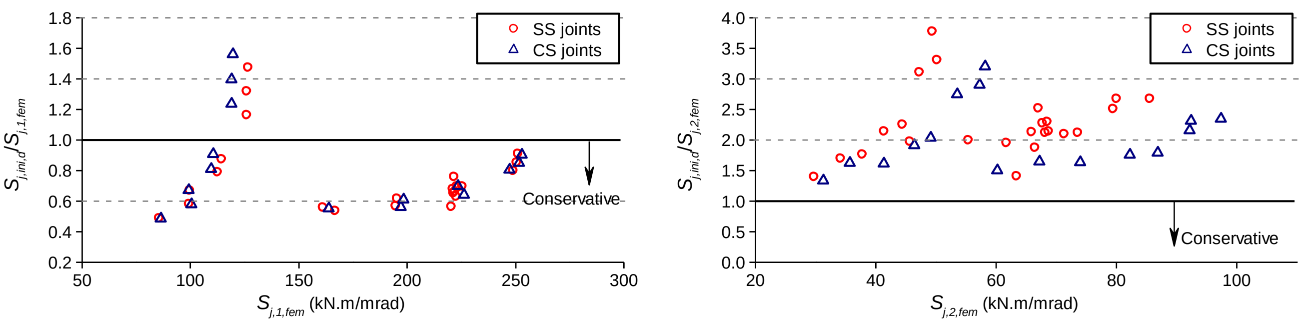

(a) First stiffness (b) Second stiffness

Fig. 20 Comparisons between design code predictions and measured first and second stiffness

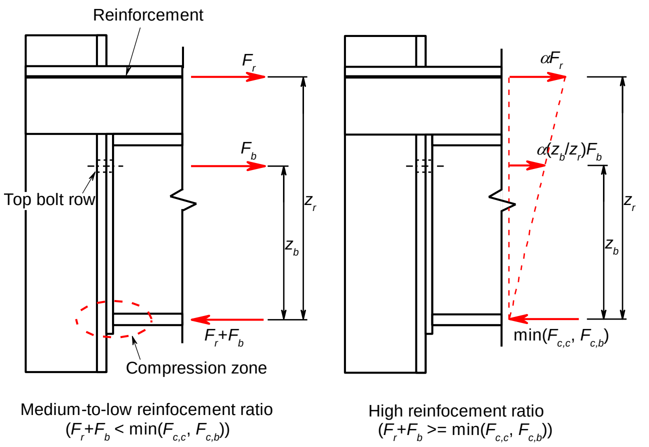

Fig. 21 Design moment carrying mechanism of composite joints

measured second stiffness $S_{j,2,fem}$ are significantly smaller than the design values, with average ratios $S_{j,ini,d}/S_{j,2,fem}$ of 2.261 and 2.033 for SS and CS joints. The significant difference between the first and the second stiffness clearly shows the influence of the uncracked concrete to the rotational stiffness of composite joints.

4.2 Plastic moment resistance

According to EC3/4 and AS/NZS 2327, the (plastic) moment resistance of a composite joint with a bolted endplate connection can be determined by

$$M_{j,R} = z_r F_r + z_b F_b \tag{5}$$

where z_b and z_r are the lever arms as defined in Section 4.1. F_r is the ultimate tension resistance of the reinforcement assuming the effective area is stressed to the yield strength. Postulating that only the top bolt row contributes to the moment resistance, its ultimate resistance F_b is the smallest of the following resistances: (1) the column web in tension; (2) the column flange in bending; (3) the endplate in bending; and (4) the beam web in tension. The resistances of these components can be calculated according to the design codes.

It should be noted that Eq. (5) only holds when the sum of F_r and F_b does not exceed the smaller resistance of (1) the column web in compression F_{cc} and (2) the beam flange and web in compression F_{cb}. Concerning the later resistance, different formulas are specified in EC3/4 and AS/NZS 2327. In EC3/4

$$F_{cb} = M_{cR}/(h - t_f) \tag{6}$$

In which M_{cR} is the moment capacity of the steel beam section, h and t_f are the depth and the flange thickness of the beam. In AS/NZS 2327, $F_{c,b}$ is equal to 1.4 times the yield resistance of the beam flange in compression

$$F_{cb} = 1.4 f_{y,b} b_f t_f \tag{7}$$

When $F_r + F_b \geq$ min (F_{cc}, F_{cb}), the resistance of the tension zone F_r and F_b shall be reduced by a factor α in order to maintain equilibrium of the internal forces, as shown in Fig. 21. Considering the top bolt row in tension as a sort of equivalent "reinforcement". An equivalent reinforcement ratio can be defined as

$$\eta_{eq} = (F_r + F_b)/\min\,(F_{cc}, F_{cb}) \tag{8}$$

Note that the concept "equivalent reinforcement ratio" herein is not the common definition related to percentage area of the reinforcing bars to the concrete slab. Instead, it is used to represent the relative relationship between the resistance of the tension zone (or equivalent "reinforcement") and the compression zone. According to this relationship, a composite beam-to-column joint can be naturally classified into one of the following two types.

(1) Medium-to-low (equivalent) reinforcement ratio ($\eta_{eq} < 1$): the tension zone of the joint is able to be stressed to its ultimate tension resistance.
(2) High reinforcement (equivalent) ratio ($\eta_{eq} \geq 1$): the resistance of the tension zone is reduced to ensure equilibrium.

For joints with medium-to-low reinforcement ratio, the moment resistance is mainly determined by the resistance of the tension zone. However, for joints with high reinforcement ratio, the moment resistance is limited by the capacity of the compression zone (beam or column in compression), which means there will be no remarkable increase in the moment resistance by increasing the resistance of the tension zone.

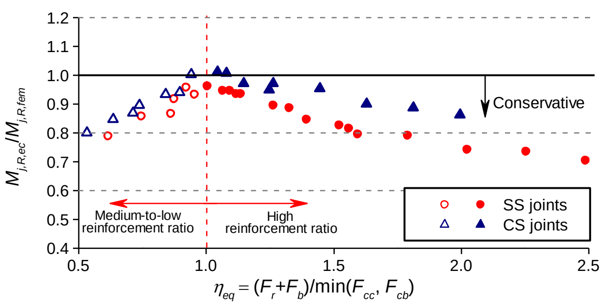

(a) EC3/4

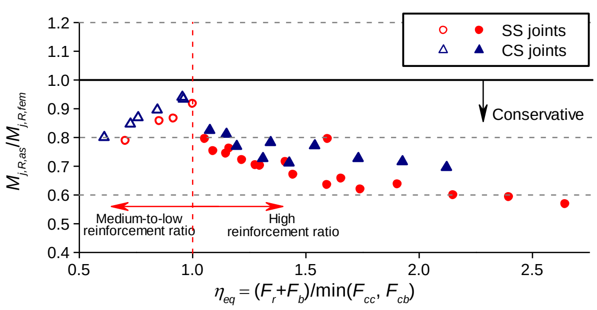

(b) AS/NZS 2327

Fig. 22 Comparisons between different design code predictions and measured moment resistances

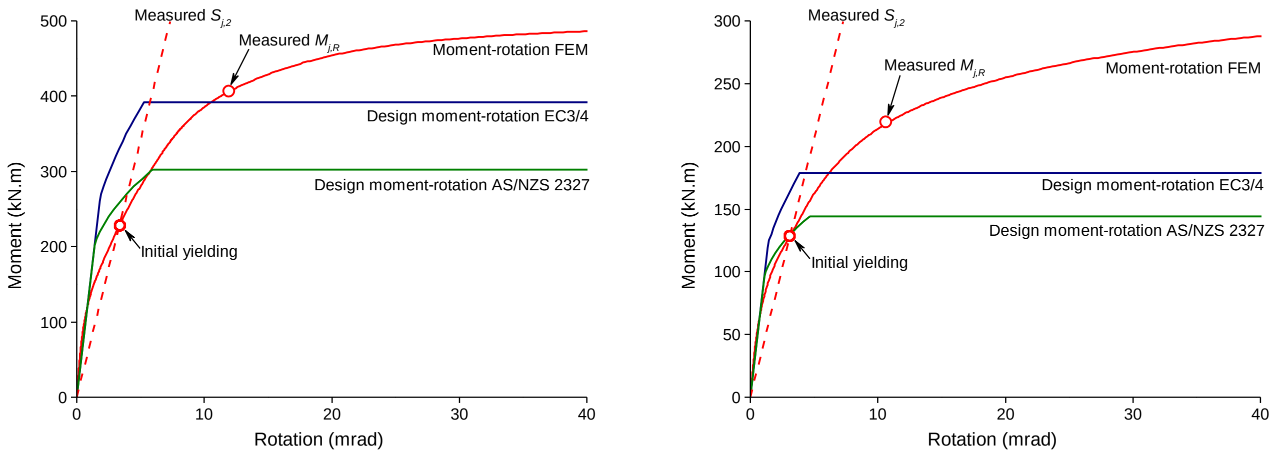

(a) CJ-SS-2 (b) CJ-SS-20

Fig. 23 Comparisons between design and measured moment-rotation characteristics

In order to appraise the predictions by design codes regarding the moment resistance, comparisons were made between the measured moment resistances and the design values as shown in Fig. 22 and Table 3. All partial safety factors were omitted in calculating the design moment resistance so that it can be compared directly with the measured values. Overall, the EC3/4 and AS/NZS 2327 underestimate the moment resistance of the SSCC joints by 12% and 28% on average. Besides, the hardening behaviour of the SSCC joints can lead to considerable increase of the moment capacity beyond the measured moment resistance, which means the design moment resistance is even more conservative as compared with the maximum moment obtained from the FE analysis. The maximum moment is underestimated by 32% and 44% on average according to EC3/4 and AS/NZS 2327, respectively.

The ratios of design-to-measured moment resistance for EC3/4 are plotted in Fig. 22 (a), with the abscissa being the equivalent reinforcement ratio defined by Eq. (8). The best agreement between the design and measured moment resistances is obtained at around η_{eq} = 1. For joints with medium-to-low reinforcement ratio (η_{eq} < 1), the design-to-measured ratio gets smaller (which means the prediction of the design code becomes more conservative) as the reinforcement ratio reduces. On the contrary, increased η_{eq} leads to smaller design-to-measured ratios for joints with η_{eq} ≥ 1 (high reinforcement ratio). Furthermore, the design prediction for SS joints is more conservative compared with that for CS joints.

The conservative prediction of the design method at both low and high (equivalent) reinforcement ratios is likely due to strain hardening of both stainless steel and carbon steel majorly resulting from the steel plates, which possess more remarkable strain hardening behaviour than the reinforcing bars or bolts (Fig. 3). Actually, in the numerical analysis, extensive levels of strain hardening were observed in SS/CS beams and endplates when the joints were loaded to their moment resistance $M_{j,R}$. This phenomenon is however neglected in the design method, as the yield strength was used in calculating the resistance of all steel components except bolts. As a result, conservative predictions are obtained, especially when the moment resistance of the joint is mainly determined by the resistance of the steel plated members (beams, columns or endplates) rather than the reinforcement. This is the case for joints with high reinforcement ratio when the moment resistance is determined by the compression resistance of the beams or columns. Similar conservative results are also expected for joints with low reinforcement ratio when the moment resistance is largely contributed by strain hardening of the equivalent T-stubs, which represent the top bolt row in tension. The effects of strain hardening can also explain the more conservative design prediction for SS joints compared with CS joints since strain hardening is more remarkable to stainless steel than carbon steel. It is noteworthy that similar effects of strain hardening have already been considered in the design of SS beams and columns through the "continuum strength method" (Gardner 2002, Afshan and Gardner 2013).

The predicted moment resistances of AS/NZS 2327 and EC3/4 are similar for joints with low reinforcement ratios. While for joints with high reinforcement ratios, the prediction of AS/NZS 2327 is more conservative than that of EC3/4. This is attributed to the lower resistance of beam flange in compression as predicted by Eq. (7) in AS/NZS 2327 compared with that specified in EC3/4 (Eq. (6)).

4.3 Design moment-rotation characteristics

According to EC3/4 and AS/NZS 2327, a composite joint can be simplified as a rotational spring connecting the beam and column, of which the behaviour can be expressed in the form of a design moment-rotation characteristic. In elastic-plastic global analysis, the design moment-rotation characteristic can be determined based on the design initial stiffness and moment resistance as defined in Section 4.1 and 4.2. The design rotational stiffness $S_{j,d}$ at an arbitrary moment $M_j \leq M_{j,R}$ is defined as

$$\begin{cases} S_{j,d} = S_{j,ini,d} \ (M_j \leq 2/3M_{j,R}) \\ S_{j,d} = S_{j,ini,d}/(1.5M_j/M_{j,R})^{\Psi} \ (2/3M_{j,R} < M_j \leq M_{j,R}) \end{cases} \quad (9)$$

where Ψ is a coefficient taken as 1.7 in EC4 and 2.7 in AS/NZS 2327. Once the moment reaches $M_{j,R}$, a perfect plastic response $M_j = M_{j,R}$ is assumed.

As shown in Fig. 23, comparisons are made between the design moment-rotation characteristics and the moment-rotation curves of SSCC joints obtained from the numerical analysis. It is obvious that the rotational stiffness of SSCC joints changes significantly at early loading stages (prior to initial yielding) due to gradual cracking of the concrete slab. The design and measured rotational stiffness agree well at the initial part, but deviate significantly as cracking grows. The design prediction generally overestimates the rotational stiffness up to the design moment resistance. Therefore, it is clear that a more rational design approach is required to estimate the rotational stiffness of SSCC joints. In accordance with the conclusion in Section 4.2, both the plastic moment resistance and the maximum moment of the SSCC joints are obviously underestimated by the design codes as shown in Fig. 23.

5. Conclusions

A numerical study has been presented in this paper regarding stainless steel-concrete composite (SSCC) beam-to-column joints with flush endplate connections, I-section columns and bolted shear connectors. Following conclusions can be drawn from the finite element modelling, the parametric study, and the comparisons with the existing design codes.

- The behaviour of stainless steel (SS) and carbon steel (CS) composite joints can be accurately simulated by the developed finite element (FE) model utilising the dynamic explicit algorithm. A sensitive analysis conducted confirms that a loading speed of 250 mm/s is appropriate to ensure the quasi-static response. It was also proofed that the present model is not sensitive to friction coefficient (at less friction coefficient from 0.2 to 0.4). Furthermore, in order to guarantee accurate simulation of the local buckling behaviour with C3D8R elements, six elements through plate thickness may be required.
- The rotational stiffness of a composite joint is significantly affected by cracking of the concrete slab. Therefore, two definitions of initial stiffness were defined in this study: the first stiffness is the actual initial stiffness before concrete cracking while the second stiffness is the secant up to the initial yielding point, which can represent the pre-yielding stiffness of the joint without the contribution of uncracked concrete. The (plastic) moment resistance of a composite joint is defined as corresponding to a secant of one-half the second stiffness on the moment-rotation curve, which is smaller than the maximum moment.
- Five types of failure modes can be identified for SSCC joints corresponding with the rotation capacity: (1) Failure of reinforcing bars; (2) failure of top-row bolts; (3) failure of shear connection; (4) local buckling of beam flange/web; and (5) local buckling of column web.
- Compared with pure SS joints, SSCC joints possess much higher capacity and stiffness attributed to the composite action. The bottom column web stiffener at the compression zone is important to ensure a sufficient development of the joint capacity, while the top stiffener at the tension zone is not necessary under symmetric hogging moments.
- From the parametric study, it can be found that the endplate thickness and the bolt diameter have no significant influence on the initial stiffness and the moment resistance. Increased endplate thickness and reduced bolt diameter will however lead to a decrease in the rotation capacity. By reducing the shear connection degree into the range of partial shear connection, the moment resistance and the initial stiffness will decrease, the rotation capacity will be significantly reduced due to early failure of the bolted shear connectors.
- The reinforcement ratio has marked influences on the initial stiffness, the moment resistance and the rotation capacity of SSCC joints. As the reinforcement ratio increases, the failure mode will gradually change from bolt failure to local buckling of beam flange/web in compression. Compared with CS composite joints, SSCC joints have slightly lower initial stiffness and moment resistance, and much higher rotation capacity when the reinforcement ratio is relatively low. However, for relatively high reinforcement ratios, SSCC joints are more susceptible to beam local buckling than CS composite joints, which may lead to lower rotation capacity.
- Comparisons were made between the numerical results and the design predictions of EC3/4 and AS/NZS 2327. The initial stiffness predicted by the design codes are generally smaller than the measured first stiffness for both SS and CS composite joints, since the contribution of uncracked concrete is not considered in the design method. However, compared with the measured second stiffness, the design method makes notably higher predictions. The measured moment resistances are generally higher than the design values due to strain-hardening of SS and CS materials. By comparing the numerical moment-rotation curves with the design moment-rotation characteristics, it is obvious that the design methods overestimate the rotational stiffness of SSCC joints and make over-conservative predictions on the moment capacity.
- According to the comparisons with the design codes, it is clear that some modifications are required for the current design methods in order to make more reasonable predictions for SSCC joints: The effects of strain-hardening should be taken into account along with a more rational estimation of the initial stiffness. For this aim, further experimental tests and numerical analysis of SSCC joints may be necessary.

Acknowledgments

The research described in this paper was financially supported by the Australian Research Council (ARC) under its Discovery Scheme (Project No: DP180100418). The first author is also supported by the Engineering and Information Technologies Research Scholarship (EITRS) and the Postgraduate Research Support Scheme (PRSS) awarded by the University of Sydney. All financial supports are gratefully acknowledged.

References

ABAQUS (2014), User's Manual, Version 6.14; Dassault Systemes Corp., Providence, RI, USA.

Afshan, S. and Gardner, L. (2013), "The continuous strength method for structural stainless steel design", *Thin-Wall. Struct.*, **68**, 42-49. https://doi.org/10.1016/j.tws.2013.02.011

Agheshlui, H., Goldsworthy, H., Gad, E. and Mirza, O. (2017), "Anchored blind bolted composite connection to a concrete filled steel tubular column", *Steel Compos. Struct., Int. J.*, **23**(1), 115-130. https://doi.org/10.12989/scs.2017.23.1.115

Anderson, D. and Najafi, A.A. (1994), "Performance of composite connections: Major axis end plate joints", *J. Constr. Steel Res.*, **31**(1), 31-57. https://doi.org/10.1016/0143-974X(94)90022-1

AS/NZS 2327 (2017), Composite steel-concrete construction for buildings; Standards Australia/Standards New Zealand, Sydney/Wellington, Australia/New Zealand.

Ataei, A., Bradford, M.A., Valipour Hamid, R. and Liu, X. (2016), "Experimental study of sustainable high strength steel flush end plate beam-to-column composite joints with deconstructable bolted shear connectors", *Eng. Struct.*, **123**, 124-140. https://doi.org/10.1016/j.engstruct.2016.05.035

Cai, Y. and Young, B. (2014), "Structural behavior of cold-formed stainless steel bolted connections", *Thin-Wall. Struct.*, **83**, 147-156. https://doi.org/10.1016/j.tws.2014.01.014

Cai, Y. and Young, B. (2018), "Bearing resistance design of stainless steel bolted connections at ambient and elevated temperatures", *Steel Compos. Struct., Int. J.*, **29**(2), 273-286. https://doi.org/10.12989/scs.2018.29.2.273

Cai, Y. and Young, B. (2019), "Experimental investigation of carbon steel and stainless steel bolted connections at different strain rates", *Steel Compos. Struct., Int. J.*, **30**(6), 551-565. https://doi.org/10.12989/scs.2019.30.6.551

CEN EN 1993-1-4:2006+A1:2015 (2015), Eurocode 3: Design of Steel Structures, Part 1-4: General rules-Supplementary rules for stainless steels; Comité Européen de Normalisation, Brussels, Belgium.

CEN EN 1993-1-8:2005 (2005), Eurocode 3: Design of Steel Structures, Part 1-8: Design of Joints; Comité Européen de Normalisation, Brussels, Belgium.

CEN EN 1994-1-1:2004 (2004), Eurocode 4: Design of Composite Steel and Concrete Structures, Part 1-1: General Rules and Rules for Buildings; Comité Européen de Normalisation, Brussels, Belgium.

CEN EN ISO 3506-1:2009 (2009), Mechanical properties of corrosion-resistant stainless steel fasteners, Part 1: Bolts, screws and studs; Comité Européen de Normalisation, Brussels, Belgium.

Dai, X.H., Lam, D. and Saveri, E. (2015), "Effect of concrete strength and stud collar size to shear capacity of demountable shear connectors", *J. Struct. Eng.*, **141**(11), 04015025. https://doi.org/10.1061/(ASCE)ST.1943-541X.0001267

Dubina, D., Ciutina, A.L. and Stratan, A. (2002), "Cyclic tests on bolted steel and composite double-sided beam-to-column joints", *Steel Compos. Struct., Int. J.*, **2**(2), 147-160. https://doi.org/10.12989/scs.2002.2.2.147

Elflah, M., Theofanous, M. and Dirar, S. (2019a), "Behaviour of stainless steel beam-to-column joints-Part 2: Numerical modelling and parametric study", *J. Constr. Steel Res.*, **152**, 194-212. https://doi.org/10.1016/j.jcsr.2018.04.017

Elflah, M., Theofanous, M., Dirar, S. and Yuan, H. (2019b), "Behaviour of stainless steel beam-to-column joints-Part 1: Experimental investigation", *J. Constr. Steel Res.*, **152**, 183-193. https://doi.org/10.1016/j.jcsr.2018.02.040

Elflah, M., Theofanous, M., Dirar, S. and Yuan, H. (2019c), "Structural behaviour of stainless steel beam-to-tubular column joints", *Eng. Struct.*, **184**, 158-175. https://doi.org/10.1016/j.engstruct.2019.01.073

El-Tawil, S.M. and Deierlein, G.G. (1996), "Fiber element analysis of composite beam-column cross-sections", Report No, 96-6; School of Civil and Environmental Engineering, Cornell Univerisity, Ithaca, NY, USA.

Gardner, L. (2002), "A new approach to structural stainless steel design", Imperial College of Science, Technology and Medicine, London, UK.

Gardner, L., Bu, Y., Francis, P., Baddoo, N.R., Cashell, K.A. and McCann, F. (2016), "Elevated temperature material properties of stainless steel reinforcing bar", *Constr. Build Mater.*, **114**, 977-997. https://doi.org/10.1016/j.conbuildmat.2016.04.009

Girão Coelho, A.M. and Bijlaard, F.S.K. (2007), "Experimental behaviour of high strength steel end-plate connections", *J. Const. Steel Res.*, **63**(9), 1228-1240. https://doi.org/10.1016/j.jcsr.2006.11.010

Han, L.-H., Xu, C.-Y. and Tao, Z. (2019), "Performance of concrete filled stainless steel tubular (CFSST) columns and joints: Summary of recent research", *J. Constr. Steel Res.*, **152**, 117-131. https://doi.org/10.1016/j.jcsr.2018.02.038

Hasan, M.J., Al-Deen, S. and Ashraf, M. (2019), "Behaviour of top-seat double web angle connection produced from austenitic stainless steel", *J. Const. Steel Res.*, **155**, 460-479. https://doi.org/10.1016/j.jcsr.2018.12.015

Kwon, G., Engelhardt, M.D. and Klingner, R.E. (2010), "Behavior of post-installed shear connectors under static and fatigue loading", *J. Const. Steel Res.*, **66**(4), 532-541. https://doi.org/10.1016/j.jcsr.2009.09.012

Leon, R.T. and Zandonini, R. (1992), *Composite Connections*, Elsevier Applied Science London.

Li, D., Huang, Z., Uy, B., Thai, H.-T. and Hou, C. (2019a), "Slenderness limits for fabricated S960 ultra-high-strength steel and composite columns", *J. Constr. Steel Res*. **159** 109-121. https://doi.org/10.1016/j.jcsr.2019.04.025

Li, D., Uy, B. and Wang, J. (2019b), "Behaviour and design of high-strength steel beam-to-column joints", *Steel Compos. Struct., Int. J.*, **31**(3), 303-317. https://doi.org/10.12989/scs.2019.31.3.303

Liew, J.Y.R., Teo, T.H., Shanmugam, N.E. and Yu, C.H. (2000), "Testing of steel–concrete composite connections and appraisal of results", *J. Constr. Steel Res.*, **56**(2), 117-150. https://doi.org/10.1016/S0143-974X(99)00099-1

Liew, J.Y.R., Teo, T.H. and Shanmugam, N.E. (2004), "Composite joints subject to reversal of loading-Part 1: experimental study", *J. Const. Steel Res.*, **60**(2), 221-246. https://doi.org/10.1016/j.jcsr.2003.08.010

Loh, H.Y., Uy, B. and Bradford, M.A. (2006a), "The effects of partial shear connection in composite flush end plate joints Part I — experimental study", *J. Constr. Steel Res.*, **62**(4), 378-390. https://doi.org/10.1016/j.jcsr.2005.07.012

Loh, H.Y., Uy, B. and Bradford, M.A. (2006b), "The effects of partial shear connection in composite flush end plate joints Part II—Analytical study and design appraisal", *J. Constr. Steel Res.*, **62**(4), 391-412. https://doi.org/10.1016/j.jcsr.2005.07.010

Mander, J.B., Priestley, M.J.N. and Park, R. (1988), "Theoretical stress-strain model for confined concrete", *J. Struct. Eng.*, **114**(8), 1804-1826. https://doi.org/10.1061/(ASCE)0733-9445(1988)114:8(1804)

Mirza, O. and Uy, B. (2011), "Behaviour of composite beam–column flush end-plate connections subjected to low-probability, high-consequence loading", *Eng. Struct.*, **33**(2), 647-662. https://doi.org/10.1016/j.engstruct.2010.11.024

Pavlović, M., Marković, Z., Veljković, M. and Buđevac, D. (2013), "Bolted shear connectors vs. headed studs behaviour in push-out tests", *J. Const. Steel Res.*, **88** 134-149. https://doi.org/10.1016/j.jcsr.2013.05.003

Rehman, N., Lam, D., Dai, X. and Ashour, A.F. (2016), "Experimental study on demountable shear connectors in composite slabs with profiled decking", *J. Const. Steel Res.*, **122**, 178-189. https://doi.org/10.1016/j.jcsr.2016.03.021

Salih, E.L., Gardner, L. and Nethercot, D.A. (2010), "Numerical investigation of net section failure in stainless steel bolted connections", *J. Constr. Steel Res.*, **66**(12), 1455-1466. https://doi.org/10.1016/j.jcsr.2010.05.012

Salih, E.L., Gardner, L. and Nethercot, D.A. (2011), "Bearing failure in stainless steel bolted connections", *Eng. Struct.*, **33**(2), 549-562. https://doi.org/10.1016/j.engstruct.2010.11.013

Salih, E.L., Gardner, L. and Nethercot, D.A. (2013), "Numerical study of stainless steel gusset plate connections", *Eng. Struct.*, **49**, 448-464. https://doi.org/10.1016/j.engstruct.2012.11.032

Salvatore, W., Bursi, O. and Lucchesi, D. (2005), "Design, testing and analysis of high ductile partial-strength steel–concrete composite beam-to-column joints", *Comput. Struct.*, **83**(28), 2334-2352. https://doi.org/10.1016/j.compstruc.2005.03.028

Shanmugam, N.E., Ng, Y.H. and Liew, J.Y.R. (2002), "Behaviour of composite haunched beam connection", *Eng. Struct.*, **24**(11), 1451-1463. https://doi.org/10.1016/S0141-0296(02)00093-7

Simoes, R., Simoes da Silva, L. and Cruz, P.J.S. (2001), "Cyclic behaviour of end-plate beam-to-column composite joints", *Steel Compos. Struct., Int. J.*, **1**(3), 355-376. https://doi.org/10.12989/scs.2001.1.3.355

Simões da Silva, L., Simões, R.D. and Cruz, P.J.S. (2001), "Experimental behaviour of end-plate beam-to-column composite joints under monotonical loading", *Eng. Struct.*, **23**(11), 1383-1409. https://doi.org/10.1016/S0141-0296(01)00054-2

Song, Y.-C., Wang, R.-P. and Li, J. (2016), "Local and post-local buckling behavior of welded steel shapes in partially encased composite columns", *Thin-Wall. Struct.*, **108**, 93-108. https://doi.org/10.1016/j.tws.2016.08.003

Song, T.-Y., Tao, Z., Razzazzadeh, A., Han, L.-H. and Zhou, K. (2017), "Fire performance of blind bolted composite beam to column joints", *J. Const. Steel Res.*, **132**, 29-42. https://doi.org/10.1016/j.jcsr.2017.01.011

Song, Y., Li, J. and Chen, Y. (2019), "Local and post-local buckling of normal/high strength steel sections with concrete infill", *Thin-Wall. Struct.*, **138**, 155-169. https://doi.org/10.1016/j.tws.2019.02.004

Tao, Z., Hassan, M.K., Song, T.-Y. and Han, L.-H. (2017), "Experimental study on blind bolted connections to concrete-filled stainless steel columns", *J. Constr. Steel Res.*, **128**, 825-838. https://doi.org/10.1016/j.jcsr.2016.10.016

Thai, H.-T. and Uy, B. (2015), "Finite element modelling of blind bolted composite joints", *J. Constr. Steel Res.*, **112**, 339-353. https://doi.org/10.1016/j.jcsr.2015.05.011

Thai, H.-T., Uy, B., Yamesri and Aslani, F. (2017a), "Behaviour of bolted endplate composite joints to square and circular CFST columns", *J. Constr. Steel Res.*, **131**, 68-82. https://doi.org/10.1016/j.jcsr.2016.12.022

Thai, H.-T., Vo, T.-P., Nguyen, T.-K. and Pham, C.H. (2017b), "Explicit simulation of bolted endplate composite beam-to-CFST column connections", *Thin-Wall. Struct.*, **119**, 749-759. https://doi.org/10.1016/j.tws.2017.07.013

Vasdravellis, G., Valente, M. and Castiglioni, C.A. (2009), "Behavior of exterior partial-strength composite beam-to-column connections: Experimental study and numerical simulations", *J. Constr. Steel Res.*, **65**(1), 23-35. https://doi.org/10.1016/j.jcsr.2008.01.034

Wang, J., Uy, B., Thai, H.-T. and Li, D. (2018a), "Behaviour and design of demountable beam-to-column composite bolted joints with extended end-plates", *J. Constr. Steel Res.*, **144**, 221-235. https://doi.org/10.1016/j.jcsr.2018.02.002

Wang, J., Zhu, H., Uy, B., Patel, V., Aslani, F. and Li, D. (2018b), "Moment-rotation relationship of hollow-section beam-to-column steel joints with extended end-plates", *Steel Compos. Struct., Int. J.*, **29**(6), 717-734. https://doi.org/10.12989/scs.2018.29.6.717

Wang, J., Uy, B. and Li, D. (2019), "Behaviour of large fabricated stainless steel beam-to-tubular column joints with extended endplates", *Steel Compos. Struct., Int. J.*, **32**(1), 141-156. https://doi.org/10.12989/scs.2019.32.1.141

Waqas, R., Uy, B. and Thai, H.-T. (2019), "Experimental and numerical behaviour of blind bolted flush endplate composite connections", *J. Constr. Steel Res.*, **153**, 179-195. https://doi.org/10.1016/j.jcsr.2018.10.012

Xiao, Y., Choo, B.S. and Nethercot, D.A. (1994), "Composite connections in steel and concrete. I. Experimental behaviour of composite beam—Column connections", *J. Constr. Steel Res.*, **31**(1), 3-30. https://doi.org/10.1016/0143-974X(94)90021-3

Xiao, Y., Zeng, L., Cui, K., Jin, S. and Chen, Y. (2017), "Experimental and analytical performance evaluation of steel beam to concrete-encased composite column with unsymmetrical steel section joints", *Steel Compos. Struct., Int. J.*, **23**(1), 17-29. https://doi.org/10.12989/scs.2017.23.1.017

Yuan, H.X., Hu, S., Du, X.X., Yang, L., Cheng, X.Y. and Theofanous, M. (2019), "Experimental behaviour of stainless steel bolted T-stub connections under monotonic loading", *J. Constr. Steel Res.*, **152**, 213-224. https://doi.org/10.1016/j.jcsr.2018.02.021

DL